The inhibitory effect of rapamycin was clearly shown to be concentration dependent (Fig. 5*B*). Therefore, we may conclude that PI3K/mTOR is the major pathway that regulates HIF-1α protein synthesis in TCR-engaged T cells.

To examine the effect of rapamycin on mRNA expression of HIF-1 target genes, T cells were exposed to either hypoxia or normoxia in the absence or presence of anti-CD3 mAb, rapamycin, and MG132 as indicated; then total cellular RNA was prepared, and mRNA expression of HIF-1 target and non-target genes was determined using RT-PCR (Fig. 6). Expression of HIF-1α mRNA was not significantly altered by either of these treatment. In contrast, expression profile of those HIF-1 target genes corresponded to that of HIF-1α protein. That is, combination of anti-CD3 mAb stimulation and either hypoxia or MG132 resulted in significant induction of ADM, GLUT-3, PGK1, VEGF mRNA expression, as well as a robust increase in HIF-1α protein expression. Induction of these mRNAs was inhibited by treatment with rapamycin in accordance with the disappearance of HIF-1α protein expression. Together, these results again indicate that TCR engagement-mediated up-regulation of HIF-1α accumulation and mRNA expression of HIF-1 target genes is rapamycin-sensitive and that protein levels of HIF-1α may, at least in part, determine the levels of mRNA expression of those genes.

We finally addressed the critical requirement of HIF-1α for mRNA expression of those HIF-1 target genes in the experiments with Jurkat cells that express constitutive active mutant of HIF-1α, CA-HIF-1α, which is a chimeric protein consisting of amino acid 1 to 396 of HIF-1α and VP-16 activation domain and escapes from oxygen-dependent degradation (Fig. 7*A*). It should be noted that, in contrast to peripheral blood T cells, hypoxic treatment is sufficient

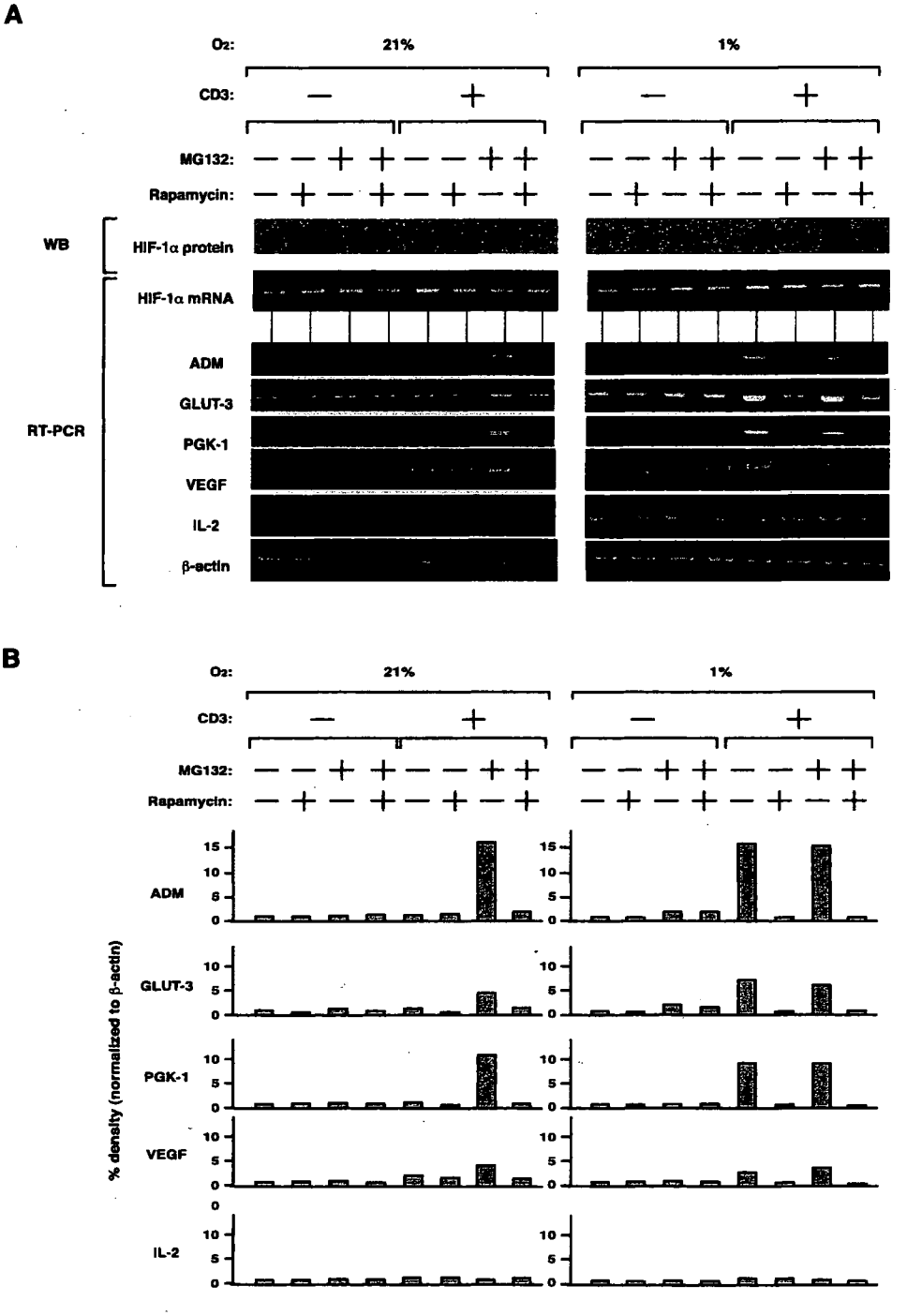

FIGURE 6. Effect of rapamycin on mRNA expression of HIF-1 target and non-target genes. Human peripheral blood T cells were cultured in the absence or presence of 5 μM MG132, 10 nM rapamycin, or 5 μg/ml immobilized anti-CD3 mAb under 21 or 1% oxygen concentration for 18 h. Protein levels of HIF-1α and mRNA levels of HIF-1α and HIF-1 target and non-target genes were determined in immunoblot and RT-PCR, respectively (*A*). Density of the bands was measured with NIH IMAGE 1.62 software being normalized to β-actin and shown in *B*. Results are shown as relative density (percentage compared with the sample without treatment (*left*) or treated with hypoxia alone (*right*)).

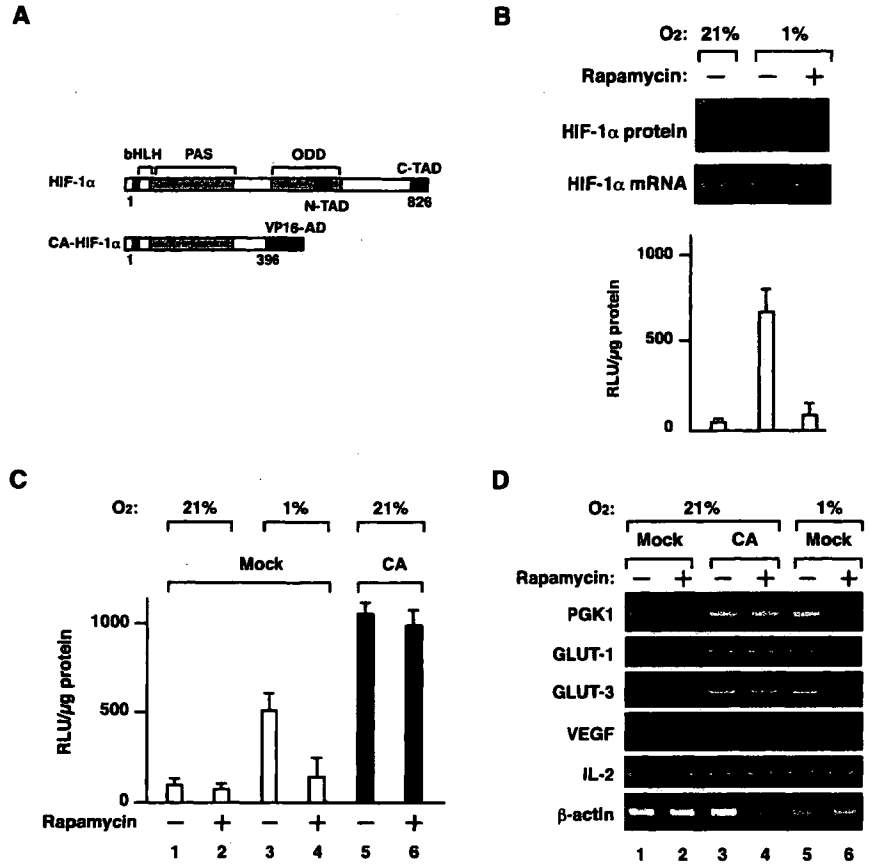

FIGURE 7. Rapamycin acts at the level of protein synthesis of HIF-1α. *A*, Schematic representation of the primary structure of the wild-type HIF-1α and CA-HIF-1α. bHLH, basic helix-loop-helix; PAS, Per/Arnt/Sim homology domain; ODD, oxygen-dependent degradation domain; N-TAD, N-terminal transactivation domain; C-TAD, C-terminal transactivation domain; VP16 AD, VP16 transactivation domain. Numbers depict positions of amino acids. *B*, Hypoxia is sufficient for HIF-1α protein expression in Jurkat cells. Jurkat cells were transfected with HRE luciferase reporter plasmids and cultured under normoxic or hypoxic condition in the presence or absence of rapamycin for 12 h; then whole cell extracts and total RNA were subjected to immunoblots for HIF-1α, luciferase assay, and RT-PCR analysis. Results of luciferase reporter gene assay were shown as relative light units (RLU) normalized to protein content and means ± SD from at least three independent experiments are presented (see *Materials and Methods*). *C*, CA-HIF-1α, bypassing oxygen-dependent degradation, acted as a constitutive transactivator. Mock-transfected (Mock) and CA-HIF-1α-transfected Jurkat cells (CA) were transfected with the HRE luciferase reporter gene and cultured in the presence or absence of 10 nM rapamycin under 21 or 1% oxygen concentration for 24 h. Cells were harvested and luciferase activity was measured. Results were shown as relative light units (RLU) normalized to protein content and means ± SD from at least three independent experiments are presented. *D*, Effect of rapamycin on mRNA expression of HIF-1 target genes in mock- and CA-HIF-1α-transfected Jurkat cells. Mock-transfected (Mock) and CA-HIF-1α-transfected Jurkat cells (CA) were cultured in the presence or absence of 10 nM rapamycin under 21 or 1% oxygen concentration for 24 h. Total RNA was prepared and RT-PCR analysis was performed to monitor mRNA expression of the indicated HIF-1 target genes (PGK,GLUT-1,GLUT-3,VEGF,) or non-HIF-1 target genes (IL-2, β-actin).

for protein expression of HIF-1α and correspondent HRE-driven reporter gene activation in parent Jurkat cells (Fig. 7*B*). Because either treatment with rapamycin (Fig. 7*B*) or serum starvation (data not shown) diminished HIF-1α expression under hypoxic conditions, it is strongly indicated that serum factors are sufficient for protein synthesis of HIF-1α in Jurkat cells in the absence of CD3 engagement as seen in many cancer cells (see introduction). Therefore, to minimize the effect of endogenous HIF-1α, we tested the effect of rapamycin in CA-HIF-1α expressing Jurkat cells under not hypoxic but normoxic conditions (Fig. 7*B*). CA-HIF-1α expressing Jurkat cells showed constitutive activation of the reporter gene expression under normoxic conditions by approximately 2-fold when compared with hypoxic parental or mock-transfected Jurkat cells, confirming that CA-HIF-1α bypassed oxygen-dependent degradation and acted as a constitutive transcriptional activator (Fig. 7, *B* and *C*). The constitutive activation of the reporter gene expression in those cells was not suppressed by rapamycin (Fig. 7*C*), indicating that constitutive active HIF-1α could bypass the inhibitory effect of rapamycin and rapamycin effects upstream of HIF-1α. Moreover, this issue was also reflected in mRNA expression profile of HIF-1α target genes. As shown in Fig. 7*D*, mRNA expression of HIF-1 target genes, PGK1, GLUT-1, GLUT-3, and VEGF in mock-transfected Jurkat cells was increased under hypoxic conditions (*lanes 1* and *5*), and markedly decreased in the presence of rapamycin again as in the case of peripheral blood T cells (*lanes 5* and *6*). In contrast, IL-2 mRNA expression was not significantly influenced in either mock-transfected or CA-HIF1 Jurkat cells. Expression of HIF-1 target genes was increased in CA-HIF-1α expressing Jurkat cells even in normoxic conditions, and the suppressive effect of rapamycin was not observed (*lanes 3* and *4*). Therefore, we may conclude that accumulation of HIF-1α protein in peripheral blood T cells is controlled by dual mechanisms: oxygen-dependent degradation and TCR-mediated synthesis involving PI3K/mTOR, and rapamycin inhibits HIF-1 target gene expression via suppression of HIF-1α synthesis.

Discussion

In this study, we suggested that hypoxia and TCR-mediated signal have distinct roles for HIF-1α expression in peripheral blood T

cells; hypoxia prevents HIF-1α protein degradation as seen in many cells, whereas TCR-mediated signal increases expression of HIF-1α protein, most possibly via enhancement of protein synthesis.

TCR ligation, either with or without CD28 engagement, stimulate PI3K followed by activation of its downstream signals including Akt (24, 25). Together with the fact that PI3K inhibitor wortmannin blocks anti-CD3-mediated HIF-1α expression, it is indicated that activation of PI3K is prerequisite for HIF-1α expression after TCR/CD3 ligation. Moreover, TCR/CD3 ligation increases HIF-1 target genes including glucose transporters and PGK1, which may be essential for supporting energy metabolisms in T cells under hypoxic conditions (26). The Pasteur effect is believed to be the most ancient metabolic adaptation to hypoxia in cells, including decreased oxidative phosphorylation and an increase in anaerobic fermentation (27–29). Because anaerobic fermentation produces far less ATP than oxidative phosphorylation per molecule of glucose, increased activity of the glycolytic pathway is necessary to maintain free ATP levels in the hypoxic cell (28). It has already been reported that HIF-1α and its target genes essentially control the metabolic state and maintain cellular ATP levels via glycolysis during hypoxia (30). Interestingly, Frauwirth et al. (31) reported that, CD3/CD28-mediated activation of PI3K has a distinct role in T cell function, regulating glucose uptake and glycolysis via enhanced expression of, for example, GLUT-1. PI3K activation after ligation of CD3 or CD3/CD28 may, therefore, converge onto the stage of protein translation of HIF-1α to potentiate protein expression of HIF-1α and maintenance of cellular ATP levels and metabolic conditions under hypoxic conditions in situ. Indeed, we have also confirmed that CD3 engagement-mediated increase in HIF-1α expression is further amplified by costimulation via CD28 (data not shown). Collectively, it should be emphasized that TCR signaling diverges into conventionally studied pathways including IL-2 production, and HIF-1-mediated metabolic adaptation, the latter of which is considered to be targeted by rapamycin.

Selective up-regulation of alternatively spliced mRNA isoform of HIF-1α was seen in Ag receptor-activated mice T cells (32). However, this is not the case in human peripheral blood T cells (22). Moreover, it is reported that, in monocyte/macrophage, lipopolysaccharides enhance HIF-1α expression via increased expression of HIF-1α mRNA (15). Hudson et al. (33) showed that rapamycin interferes with HIF-1α activation in hypoxic PC-3 cells by increasing the rate of HIF-1α degradation. Collectively, HIF-1α protein expression might be regulated via distinct mechanisms or pathways in each species, tissue or cell in a spatial- and signal-dependent manner, enabling their rationale adaptation.

Recently, involvement of PI3K/mTOR pathway in HIF-1α synthesis has been described in many cancers. In addition, rapamycin is shown to repress HIF-1α synthesis and expression of HIF-1 target genes including VEGF in these cells via targeting mTOR. Therefore, rapamycin is now considered to act as an antineoplastic agent, as well as an immunosuppressant (18, 34). It appears to be obvious to hypothesize that rapamycin suppresses HIF-1α protein expression in T cells as well. Indeed, we clearly showed that rapamycin dose-dependently decreased HIF-1α expression in CD3-engaged T cells under hypoxic conditions. Moreover, we have shown that rapamycin represses mRNA expression of HIF-1 target genes including PGK1, and GLUTs, which serve as key molecules for glycolysis, as well as that of VEGF. It should be noted that mRNA expression of, for example, IL-2 was reported not to be susceptible to treatment with rapamycin (35). Since the promoter region of the IL-2 gene does not contain HRE, we may conclude that rapamycin rather selectively targets HRE-containing genes and elicits distinct immunosuppression via, at least in part, repression of HIF-1-dependent gene expression (35).

HIF-1α has been shown to be expressed in various inflammatory diseases including Crohn's disease (36), ulcerative colitis (36), and rheumatoid arthritis (22, 37, 38), and expression of those genes is critical for adequate immune response in T cells (see Introduction). TCR-driven activation of PI3K/mTOR and HIF-1α synthesis could be an interesting target for immune modulation, and rapamycin could be one of the exploratory drugs attacking this pathway. On the other hand, classic cytotoxic drugs may have increased risk of secondary neoplasms (39–41). Considering that rapamycin may operate as an antineoplastic agent via, for example, inhibition of VEGF expression in various cancers, it is indicated that rapamycin and its analogues constitute a unique class of immunosuppressive agents from the viewpoint of not only its mechanism of actions but also distinct clinical benefit.

Acknowledgments

We are grateful to all the members of the Morimoto laboratory for fruitful discussion.

Disclosures

The authors have no financial conflict of interest.

References

1. Westermann, J., and U. Bode. 1999. Distribution of activated T cells migrating through the body: a matter of life and death. *Immunol. Today* 20: 302–306.
2. Vaupel, P., O. Thews, D. K. Kelleher, and M. Hoeckel. 1998. Current status of knowledge and critical issues in tumor oxygenation: results from 25 years research in tumor pathophysiology. *Adv. Exp. Med. Biol.* 454: 591–602.
3. Krauss, S., M. D. Brand, and F. Buttgereit. 2001. Signaling takes a breath–new quantitative perspectives on bioenergetics and signal transduction. *Immunity* 15: 497–502.
4. Semenza, G. L. 2004. Hydroxylation of HIF-1: oxygen sensing at the molecular level. *Physiology (Bethesda)* 19: 176–182.
5. Poellinger, L., and R. S. Johnson. 2004. HIF-1 and hypoxic response: the plot thickens. *Curr. Opin. Genet. Dev.* 14: 81–85.
6. Kojima, H., H. Gu, S. Nomura, C. C. Caldwell, T. Kobata, P. Carmeliet, G. L. Semenza, and M. V. Sitkovsky. 2002. Abnormal B lymphocyte development and autoimmunity in hypoxia-inducible factor 1α-deficient chimeric mice. *Proc. Natl. Acad. Sci. USA* 99: 2170–2174.
7. Cramer, T., Y. Yamanishi, B. E. Clausen, I. Forster, R. Pawlinski, N. Mackman, V. H. Haase, R. Jaenisch, M. Corr, V. Nizet, et al. 2003. HIF-1α is essential for myeloid cell-mediated inflammation. *Cell* 112: 645–657.
8. Schofield, C. J., and P. J. Ratcliffe. 2004. Oxygen sensing by HIF hydroxylases. *Nat. Rev. Mol. Cell Biol.* 5: 343–354.
9. Zelzer, E., Y. Levy, C. Kahana, B. Z. Shilo, M. Rubinstein, and B. Cohen. 1998. Insulin induces transcription of target genes through the hypoxia-inducible factor HIF-1α/ARNT. *EMBO J.* 17: 5085–5094.
10. Bilton, R. L., and G. W. Booker. 2003. The subtle side to hypoxia inducible factor (HIFα) regulation. *Eur. J. Biochem.* 270: 791–798.
11. Zhong, H., K. Chiles, D. Feldser, E. Laughner, C. Hanrahan, M. M. Georgescu, J. W. Simons, and G. L. Semenza. 2000. Modulation of hypoxia-inducible factor 1α expression by the epidermal growth factor/phosphatidylinositol 3-kinase/PTEN/AKT/FRAP pathway in human prostate cancer cells: implications for tumor angiogenesis and therapeutics. *Cancer Res.* 60: 1541–1545.
12. Laughner, E., P. Taghavi, K. Chiles, P. C. Mahon, and G. L. Semenza. 2001. HER2 (neu) signaling increases the rate of hypoxia-inducible factor 1α (HIF-1α) synthesis: novel mechanism for HIF-1-mediated vascular endothelial growth factor expression. *Mol. Cell Biol.* 21: 3995–4004.
13. Fukuda, R., K. Hirota, F. Fan, Y. D. Jung, L. M. Ellis, and G. L. Semenza. 2002. Insulin-like growth factor 1 induces hypoxia-inducible factor 1-mediated vascular endothelial growth factor expression, which is dependent on MAP kinase and phosphatidylinositol 3-kinase signaling in colon cancer cells. *J. Biol. Chem.* 277: 38205–38211.
14. Alam, H., E. T. Maizels, Y. Park, S. Ghaey, Z. J. Feiger, N. S. Chandel, and M. Hunzicker-Dunn. 2004. Follicle-stimulating hormone activation of hypoxia-inducible factor-1 by the phosphatidylinositol 3-kinase/AKT/Ras homolog enriched in brain (Rheb)/mammalian target of rapamycin (mTOR) pathway is necessary for induction of select protein markers of follicular differentiation. *J. Biol. Chem.* 279: 19431–19440.
15. Blouin, C. C., E. L. Page, G. M. Soucy, and D. E. Richard. 2004. Hypoxic gene activation by lipopolysaccharide in macrophages: implication of hypoxia-inducible factor 1α. *Blood* 103: 1124–1130.
16. Masri, M. A. 2003. The mosaic of immunosuppressive drugs. *Mol. Immunol.* 39: 1073–1080.
17. Hay, N., and N. Sonenberg. 2004. Upstream and downstream of mTOR. *Genes Dev.* 18: 1926–1945.

18. Guba, M., C. Graeb, K. W. Jauch, and E. K. Geissler. 2004. Pro- and anti-cancer effects of immunosuppressive agents used in organ transplantation. *Transplantation* 77: 1777–1782.
19. Huang, S., and P. J. Houghton. 2003. Targeting mTOR signaling for cancer therapy. *Curr. Opin. Pharmacol.* 3: 371–377.
20. Guba, M., P. von Breitenbuch, M. Steinbauer, G. Koehl, S. Flegel, M. Hornung, C. J. Bruns, C. Zuelke, S. Farkas, M. Anthuber, et al. 2002. Rapamycin inhibits primary and metastatic tumor growth by antiangiogenesis: involvement of vascular endothelial growth factor. *Nat. Med.* 8: 128–135.
21. Majumder, P. K., P. G. Febbo, R. Bikoff, R. Berger, Q. Xue, L. M. McMahon, J. Manola, J. Brugarolas, T. J. McDonnell, T. R. Golub, et al. 2004. mTOR inhibition reverses Akt-dependent prostate intraepithelial neoplasia through regulation of apoptotic and HIF-1-dependent pathways. *Nat. Med.* 10: 594–601.
22. Makino, Y., H. Nakamura, E. Ikeda, K. Ohnuma, K. Yamauchi, Y. Yabe, L. Poellinger, Y. Okada, C. Morimoto, and H. Tanaka. 2003. Hypoxia-inducible factor regulates survival of antigen receptor-driven T cells. *J. Immunol.* 171: 6534–6540.
23. Kodama, T., N. Shimizu, N. Yoshikawa, Y. Makino, R. Ouchida, K. Okamoto, T. Hisada, H. Nakamura, C. Morimoto, and H. Tanaka. 2003. Role of the glucocorticoid receptor for regulation of hypoxia-dependent gene expression. *J. Biol. Chem.* 278: 33384–33391.
24. Okkenhaug, K., and B. Vanhaesebroeck, B. 2003. PI3K in lymphocyte development, differentiation and activation. *Nat. Rev. Immunol.* 3: 317–330.
25. Ward, S. G., and D. A. Cantrell. 2001. Phosphoinositide 3-kinases in T lymphocyte activation. *Curr. Opin. Immunol.* 13: 332–338.
26. MacDonald, H. R., and C. J. Koch. 1977. Energy metabolism and T-cell-mediated cytolysis. I. Synergism between inhibitors of respiration and glycolysis. *J. Exp. Med.* 146: 698–709.
27. Pasteur, L. 1861. Experience et vues nouvelles sur la nature des fermentations. *Comp. Rend. Acad. Sci.* 52: 1260.
28. Stryer, L. 1995. *Biochemistry*, 4th ed, New York.
29. Hardie, D. G. 2000. Metabolic control: a new solution to an old problem. *Curr. Biol.* 10: R757–R759.
30. Seagroves, T. N., H. E. Ryan, H. Lu, B. G. Wouters, M. Knapp, P. Thibault, K. Laderoute, and R. S. Johnson. 2001. Transcription factor HIF-1 is a necessary mediator of the pasteur effect in mammalian cells. *Mol. Cell Biol.* 21: 3436–3444.
31. Frauwirth, K. A., J. L. Riley, M. H. Harris, R. V. Parry, J. C. Rathmell, D. R. Plas, R. L. Elstrom, C. H. June, and C. B. Thompson. 2002. The CD28 signaling pathway regulates glucose metabolism. *Immunity* 16: 769–777.
32. Lukashev, D., C. Caldwell, A. Ohta, P. Chen, and M. Sitkovsky. 2001. Differential regulation of two alternatively spliced isoforms of hypoxia-inducible factor-1α in activated T lymphocytes. *J. Biol. Chem.* 276: 48754–48763.
33. Hudson, C. C., M. Liu, G. G. Chiang, D. M. Otterness, D. C. Loomis, F. Kaper, A. J. Giaccia, and R. T. Abraham. 2002. Regulation of hypoxia-inducible factor 1α expression and function by the mammalian target of rapamycin. *Mol. Cell Biol.* 22: 7004–7014.
34. Hidalgo, M., and E. K. Rowinsky, E. K. 2000. The rapamycin-sensitive signal transduction pathway as a target for cancer therapy. *Oncogene* 19: 6680–6686.
35. Matsue, H., C. Yang, K. Matsue, D. Edelbaum, M. Mummert, and A. Takashima. 2002. Contrasting impacts of immunosuppressive agents (rapamycin, FK506, cyclosporin A, and dexamethasone) on bidirectional dendritic cell-T cell interaction during antigen presentation. *J. Immunol.* 169: 3555–3564.
36. Giatromanolaki, A., E. Sivridis, E. Maltezos, D. Papazoglou, C. Simopoulos, K. C. Gatter, A. L. Harris, and M. I. Koukourakis. 2003. Hypoxia inducible factor 1α and 2α overexpression in inflammatory bowel disease. *J. Clin. Pathol.* 56: 209–213.
37. Giatromanolaki, A., E. Sivridis, E. Maltezos, N. Athanassou, D. Papazoglou, K. C. Gatter, A. L. Harris, and M. I. Koukourakis. 2003. Upregulated hypoxia inducible factor-1alpha and -2alpha pathway in rheumatoid arthritis and osteoarthritis. *Arthritis Res. Ther.* 5: R193–R201.
38. Hollander, A. P., K. P. Corke, A. J. Freemont, and C. E. Lewis. 2001. Expression of hypoxia-inducible factor 1α by macrophages in the rheumatoid synovium: implications for targeting of therapeutic genes to the inflamed joint. *Arthritis Rheum.* 44: 1540–1544.
39. Penn, I. 1998. Occurrence of cancers in immunosuppressed organ transplant recipients. *Clin. Transpl.* 1998: 147–158.
40. Garver, R. I., Jr., G. L. Zorn, X. Wu, D. C. McGiffin, K. R. Young, Jr., and N. B. Pinkard. 1999. Recurrence of bronchioloalveolar carcinoma in transplanted lungs. *N. Engl. J. Med.* 340: 1071–1074.
41. Euvrard, S., C. Ulrich, and N. Lefrancois. 2004. Immunosuppressants and skin cancer in transplant patients: focus on rapamycin. *Dermatol. Surg.* 30: 628–633.

HEXIM1 forms a transcriptionally abortive complex with glucocorticoid receptor without involving 7SK RNA and positive transcription elongation factor b

Noriaki Shimizu*, Rika Ouchida*, Noritada Yoshikawa*, Tetsuya Hisada*, Hajime Watanabe†, Kensaku Okamoto*, Masatoshi Kusuhara‡, Hiroshi Handa§, Chikao Morimoto*, and Hirotoshi Tanaka*¶

*Division of Clinical Immunology and Department of Rheumatology and Allergy, Institute of Medical Science, University of Tokyo, 4-6-1, Shirokanedai, Minato-ku, Tokyo 108-8639, Japan; †Department of Environmental Biology, National Institute for Basic Biology, National Institutes of Natural Science, Okazaki 444-8787, Japan; ‡Internal Medicine I, National Defense Medical College, Tokorozawa 359-8513, Japan; and §Graduate School of Bioscience and Biotechnology, Tokyo Institute of Technology, Yokohama 226-8501, Japan

Edited by Jan-Åke Gustafsson, Karolinska Institute, Huddinge, Sweden, and approved April 28, 2005 (received for review December 30, 2004)

The HEXIM1 protein has been shown to form a protein–RNA complex composed of 7SK small nuclear RNA and positive transcription elongation factor b (P-TEFb), which is composed of cyclin-dependent kinase 9 (CDK9) and cyclin T1, and to inhibit the kinase activity of CDK9, thereby suppressing RNA polymerase II-dependent transcriptional elongation. Here, we biochemically demonstrate that HEXIM1 forms a distinct complex with glucocorticoid receptor (GR) without RNA, CDK9, or cyclin T1. HEXIM1, through its arginine-rich nuclear localization signal, directly associates with the ligand-binding domain of GR. Introduction of HEXIM1 short interfering RNA and adenovirus-mediated exogenous expression of HEXIM1 positively and negatively modulated glucocorticoid-responsive gene activation, respectively. In the nucleus, HEXIM1 was shown to localize in a distinct compartment from that of the p160 coactivator transcriptional intermediary factor 2. Overexpression of HEXIM1 decreased ligand-dependent association between GR and transcriptional intermediary factor 2. Antisense-mediated disruption of 7SK blunted the negative effect of HEXIM1 on arylhydrocarbon receptor-dependent transcription but not on GR-mediated one, indicating that a class of transcription factors are direct targets of HEXIM1. These results indicate that HEXIM1 has dual roles in transcriptional regulation: inhibition of transcriptional elongation dependent on 7SK RNA and positive transcription elongation factor b and interference with the sequence-specific transcription factor GR via a direct protein–protein interaction. Moreover, the fact that the central nuclear localization signal of HEXIM1 is essential for both of these actions may argue the crosstalk of these functions.

nuclear receptor | RNA-binding protein | ribonucleoprotein | steroid | nuclear localization signal

Transcription is a complex multistep process that relies on highly coordinated actions of a number of cis- and trans-acting elements (1–3). RNA polymerase II (RNAP II), as the central player in transcription of class II genes, carries out a series of events that include promoter binding, transcription initiation, promoter escape, transcription elongation, and transcription termination. During transcription by RNAP II, phosphorylation of the C-terminal domain of the largest subunit of RNAP II by positive transcription elongation factor b (P-TEFb), which is composed of cyclin-dependent kinase 9 (CDK9) and cyclin T1, is crucial for the transition from the abortive to the productive phase of transcriptional elongation, leading to the generation of full-length RNA transcripts. P-TEFb has been shown to lose its ability to phosphorylate the C-terminal domain when associated with 7SK RNA, a 330-nt small nuclear RNA (4–6).

HEXIM1 was first identified as a protein whose expression is induced in vascular smooth muscle cells (VSMC) in response to hexamethylene bisacetamide (HMBA) treatment (7, 8). The HEXIM1 protein consists of 359 amino acids and is tentatively divided into three regions: an N-terminal proline-rich region (amino acids 1–149), a lysine-arginine rich central nuclear localization signal (NLS)-like region (amino acids 150–177), and a C-terminal acidic region enriched in aspartic and glutamic acid residues (amino acids 178–359) (8). Recently, HEXIM1 was shown to bind 7SK via the NLS, which is considered to be an arginine-rich RNA-binding motif, to form a complex with P-TEFb and to potently and specifically inhibit the kinase and transcriptional activities of P-TEFb (9–12). Roughly half of nuclear P-TEFb in HeLa cells is considered to be sequestered in an inactive state with 7SK and HEXIM1. However, this population of P-TEFb can be rapidly dissociated from 7SK and HEXIM1 upon various treatment of cells, some of which in turn cause the stimulation of C-terminal domain phosphorylation and global increase in RNA and protein synthesis (9, 10, 13, 14). It is therefore of particular importance to address how association of HEXIM1 with 7SK and P-TEFb is controlled. On the contrary, HEXIM1 appears to be in large excess over P-TEFb (11). Moreover, it has recently been reported that HEXIM1 might interact with cellular factors other than 7SK/P-TEFb and perform distinct functions (15). Interestingly, a hypothetical protein gene located in a locus adjacent to that of HEXIM1 has a great sequence similarity to HEXIM1. This protein, named HEXIM2, was recently shown to be expressed in testes and to have an elongation-suppressive function as well (16, 17). For further understanding of the role of HEXIMs in transcriptional regulation and gene expression, it is therefore essential to identify partner factors of HEXIMs.

In the present study, we demonstrate that HEXIM1 forms a distinct complex with the glucocorticoid receptor (GR) in an RNA-independent fashion. GR is a classical member of the nuclear receptor superfamily and has a modular structure consisting of the N-terminal transactivating domain [also termed activation function-1 (AF1)], the central DNA-binding domain (DBD), and the C-terminal ligand-binding domain (LBD), and AF2 at the C terminus (18, 19). It is believed that, upon ligand binding, GR translocates into the nucleus and binds to a target DNA sequence, thereby activating transcription via complex interplay with coactivators, mediators, and target DNA (18, 19). HEXIM1, through its arginine-rich NLS, directly associates with the GR LBD and appears to interfere with productive commu-

This paper was submitted directly (Track II) to the PNAS office.

Abbreviations: GR, glucocorticoid receptor; DBD, DNA-binding domain; LBD, ligand binding domain; P-TEFb, positive transcription elongation factor b; NLS, nuclear localization signal; AhR, arylhydrocarbon receptor; VSMC, vascular smooth muscle cells; HMBA, hexamethylene bisacetamide; TIF2, transcriptional intermediary factor 2; CDK9, cyclin-dependent kinase 9; AF1, activation function-1; DEX, dexamethasone.

¶To whom correspondence should be addressed. E-mail: hirotnk@ims.u-tokyo.ac.jp.

nication of GR with the p160 coactivator transcriptional intermediary factor 2 (TIF2). These results indicate that HEXIM1 has dual roles in transcriptional regulation by means of a single arginine-rich domain: inhibition of transcriptional elongation dependent on 7SK RNA and P-TEFb and interference with GR by a direct protein–protein interaction.

Materials and Methods

Recombinant DNA, Antibodies, and Cells. Expression plasmids for FLAG-tagged and GST-fused wild-type and mutant HEXIM1 were described in ref. 8. pGEX/hHEXIM1/Δ150–177+SV, pGEX/hHEXIM1/150–180, pCMX/6His-GR, and its mutants were generated by cloning appropriate PCR fragments into pGEX6P-3 (Amersham Biosciences) or pCMX (20). Expression plasmids for double-stranded hairpin RNAs were constructed from pSilencer3.1-H1 neo (Ambion, Austin, TX). The target sequence used was 5′-gaagaagcggcattggaaa-3′ for HEXIM1. Recombinant adenovirus encoding FLAG- and 6His-HEXIM1 (AdCALNL/FHhHEXIM1) was generated by using an Adenovirus Cre/loxP-regulated Expression Vector set (TaKaRa). The following antibodies were used in this study: GR, TIF2 (catalog nos. 611227 and 610985, respectively, BD Transduction Laboratories), CDK9, cyclinT1, CBP (catalog nos. sc-484G, sc-8127, and sc-369, respectively, Santa Cruz Biotechnology), FLAG, α-actinin (catalog nos. F3165 and A5044, respectively, Sigma), arylhydrocarbon receptor (AhR; catalog no. SA-210, Biomol, Plymouth Meeting, PA), and HEXIM1 (8). HeLa, COS7, and HepG2 cells were obtained from RIKEN Cell Bank (Tsukuba, Japan) and cultured in DMEM (Sigma) supplemented with steroid-stripped 10% FBS (21). Human VSMC were obtained from Kurabo (Osaka, Japan) and maintained as described in ref. 8.

Transfection and Luciferase Assay. Cells (1.5×10^5) were transfected in six-well plates with 500 ng of glucocorticoid-responsive luciferase reporter plasmid (GRE-Luc) or xenobiotic-responsive luciferase reporter plasmid using TransIt-LT1 (Panvera, Madison, WI) (22). After treatment with dexamethasone (DEX) (Sigma) or 3-methylchoranthrene (Sigma) for 24 h, cellular luciferase activity was measured by using a luciferase assay system (Promega). For cotransfection assay with plasmids and antisense 7SK deoxyoligonucleotide, Lipofectamine reagent and Plus reagent (Invitrogen) were used. The deoxyoligonucleotide sequences used were 5′-ccttgagagcttgtttggagg-3′ for antisense 7SK and 5′-cgtcgatgtgatgctgtgtga-3′ for scrambled deoxyoligonucleotide (14).

Affinity Purification and Mass Spectrometry. Bacterially expressed GST-HEXIM1 proteins were immobilized onto glutathione Sepharose 4B resin (Amersham Biosciences). HeLa cell nuclear extracts prepared as described in ref. 23 were incubated with the affinity beads for 1.5 h at 4°C and washed with binding buffer (10 mM Hepes, pH 7.9/10% glycerol/50 mM KCl/6 mM $MgCl_2$/0.1 mM EDTA/0.5 mM DTT/0.5 mM PMSF/0.1% Nonidet P-40). The bound proteins were eluted with elution buffer (10 mM Hepes, pH 7.9/10% glycerol/1 M NaCl/0.1 mM EDTA/0.5 mM DTT/0.5 mM PMSF/0.1% Nonidet P-40) and separated by 5–20% SDS/PAGE, and the amino acid sequence was determined by mass spectrometry as described in ref. 24.

Indirect Immunofluorescence. Cells were plated on coverslips, fixed in 3.7% paraformaldehyde for 20 min at room temperature, permeabilized with 0.1% Triton X-100 in PBS for 15 min, and incubated with blocking buffer (3% BSA/0.1% Triton X-100 in PBS) for 1 h. Cells were incubated for 1 h with primary antibodies and stained with Alexa Fluor 594- or 488-conjugated secondary antibodies (Molecular Probes). Cellular fluorescence was analyzed with Olympus laser scanning confocal microscopy. For digital image analysis, Olympus FLUOVIEW software was used as described in ref. 25.

GST Pull-Down Assays and Immunoprecipitations. 6His-GR and its mutants were *in vitro*-translated with [^{35}S]methionine by using TNT Coupled Reticulocyte Lysate systems (Promega) and incubated for 1.5 h with GST-HEXIM1 immobilized beads. Bound proteins were eluted with sample buffer, separated by SDS/PAGE, and detected by fluorography. For immunoprecipitation, HeLa cell whole-cell extracts (500 μg) were prepared in radioimmunoprecipitation assay buffer (10 mM Tris, pH 7.9/150 mM NaCl/0.1% SDS/1% Triton X-100/1% deoxycholate/1 mM DTT/1 mM PMSF), incubated with 5 μg of anti-HEXIM1 or anti-CDK9 antibody for 1.5 h with or without RNase A, and incubated with protein A-Sepharose (Amersham Biosciences) for 1.5 h. HeLa cell nuclear extracts (200 μg) were prepared as described in ref. 26, incubated with 1 μg of anti-TIF2 antibody for 6 h in immunoprecipitation buffer (20 mM Hepes, pH 7.9/50 mM NaCl/1 mM EDTA/1 mM EGTA/0.1% Nonidet P-40/1 mM DTT/1 mM PMSF/10 μM DEX), and incubated with Protein G-Sepharose (Amersham Biosciences) for 1.5 h. Bound proteins were resolved by SDS/PAGE followed by Western blotting.

RT-PCR and DNA Microarray. Reverse transcription was performed by using SuperScript II (Invitrogen). Specific primers for PCR are described elsewhere (8, 27–29). Total RNA of HepG2 cells was prepared as recommended by Affymetrix. Samples were run by using a GeneChip Human Genome Focus Array (Affymetrix, Santa Clara, CA) comprising 8,746 probe sets representing ≈8,400 human genes. Genes whose expression was significantly detected at any time point were considered to be valid for further analysis, and 5,288 genes were analyzed by using GENECHIP software (Affymetrix) as described in ref. 30.

Results

Complex Formation of HEXIM1 with GR Independent of RNA and P-TEFb. HEXIM1-binding proteins were affinity-purified by using GST-HEXIM1 and identified with mass spectrometry. In the absence of treatment with RNase A, HEXIM1 bound numerous proteins participating in RNA metabolism, probably because of its RNA-binding property (data not shown). In clear contrast, in the presence of an excess of RNase A, we detected a single HEXIM1-binding protein with a molecular weight of 94 kDa (Fig. 1*A*). Mass spectrometric analysis revealed that the protein is GR. Western blot analysis showed that eluates from HEXIM1 affinity beads contained CDK9 and cyclin T1, both of which were diminished in the presence of RNase A (Fig. 1*B*). In contrast, RNase A did not affect the interaction between HEXIM1 and GR (Fig. 1*B*). Immunoprecipitation of HeLa whole-cell extracts with anti-HEXIM1 antibody demonstrated that HEXIM1 forms distinct complexes with P-TEFb and GR in RNA-dependent and -independent manners, respectively (Fig. 1*C*). Because samples immunoprecipitated from the extracts with anti-CDK9 antibody contained HEXIM1 but not GR (Fig. 1*D*), we concluded that HEXIM1 forms at least two protein complexes, one involving P-TEFb and 7SK and the other containing GR. We also concluded that the interaction between HEXIM1 and GR does not require RNA.

HEXIM1 Negatively Modulates Glucocorticoid-Mediated Gene Expression. Adenovirus-mediated overexpression of HEXIM1 in HepG2 cells decreased DEX-induced mRNA expression of endogenous glucocorticoid-regulated genes without significant alteration in GR protein levels in whole-cell extracts (Fig. 2*A*). DNA microarray analysis revealed that expression of 2.5% of the 5,288 annotated genes was repressed by the exogenous FLAG-HEXIM1, possibly because of the inhibition of P-TEFb. Con-

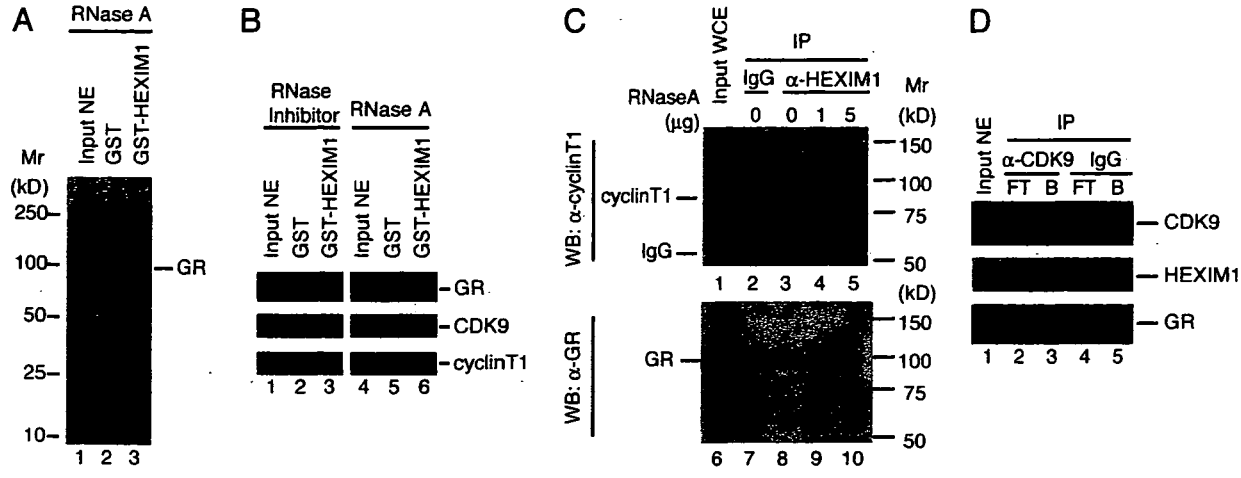

Fig. 1. HEXIM1 forms a distinct complex with GR independent of RNA and P-TEFb. (*A* and *B*) Identification of GR as a HEXIM1-binding protein. Nuclear extracts (NE) from HeLa cells were incubated with GST or GST-HEXIM1 immobilized beads. Bound fractions were analyzed with SDS/PAGE followed by silver staining (*A*) and analyzed on Western blots (WB) (*B*). (*C* and *D*) HEXIM1-GR complex does not contain 7SK RNA, CDK9, or cyclin T1. Whole-cell extracts (WCE) (*C*) or nuclear extracts (*D*) from HeLa cells were immunoprecipitated with anti-HEXIM1 (*C*) or anti-CDK9 (*D*) antibodies in the absence or presence of RNase A. Immunocomplexes were analyzed on Western blots as indicated. IP, immunoprecipitation; FT, flow through; B, bound.

cerning glucocorticoid-regulated genes, 135 genes (2.6% of total) were positively regulated by DEX, and the induction responses of 125 genes (92.6% of 135 genes) were canceled in the presence of exogenous FLAG-HEXIM1 (Fig. 2*B*; see also Table 1, which is published as supporting information on the PNAS web site). Short interfering RNA-mediated knockdown of HEXIM1 did not influence total amounts of GR (data not shown) but enhanced GR-dependent reporter gene expression, which was again canceled by exogenous expression of FLAG-HEXIM1 (Fig. 2*C*). These results indicate the negative regulatory role of HEXIM1 in GR-mediated transcription. In concert with this idea, treatment of VSMC with HMBA, which resulted in enhancement of HEXIM1 protein expression (8), decreased GR-dependent transcription (Fig. 2*D*).

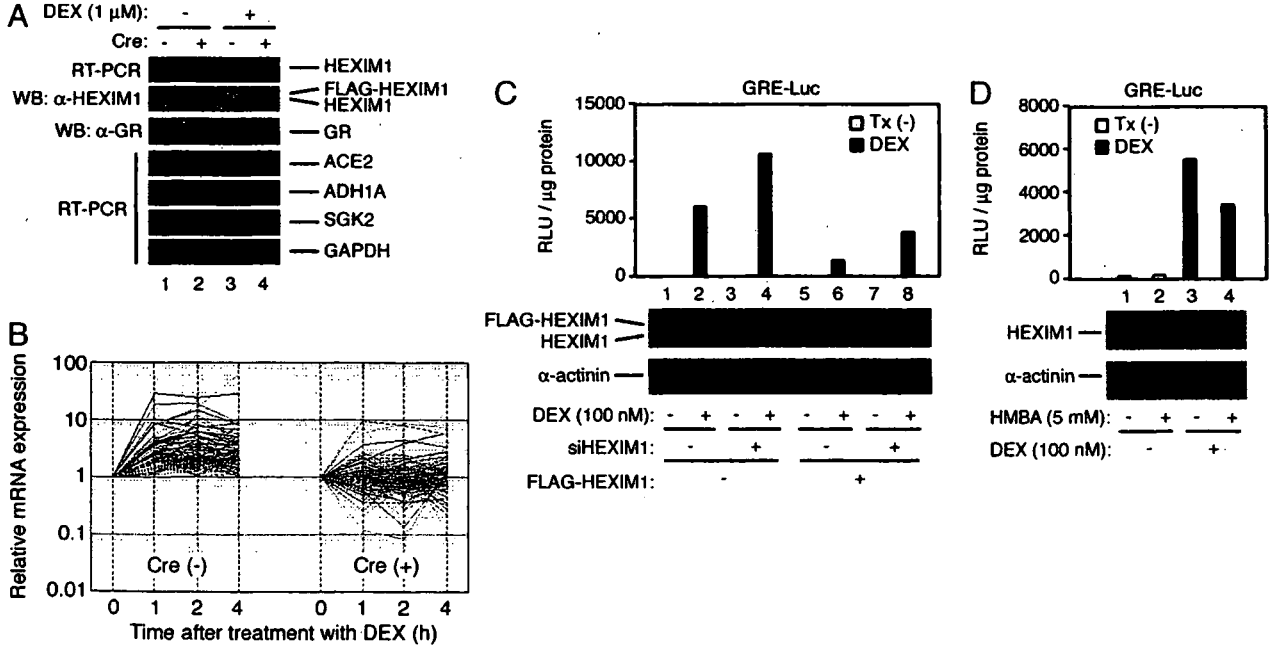

Fig. 2. Effects of HEXIM1 on glucocorticoid-mediated gene expression. (*A*) HepG2 cells were infected with a recombinant adenovirus carrying loxP-flanked FLAG-HEXIM1 cDNA (AdCALNL/FHhHEXIM1; multiplicity of infection = 30) alone (Cre −) or along with a recombinant adenovirus expressing Cre recombinase (Cre +). After a 2-h treatment with 1 μM DEX, mRNA and protein expression levels were analyzed with RT-PCR and Western blots (WB), respectively. ACE2, angiotensin I converting enzyme 2; ADH1A, alcohol dehydrogenase 1A; SGK2, serum/glucocorticoid-regulated kinase 2. (*B*) HepG2 cells were infected with these recombinant adenoviruses and cultured in the presence of 1 μM DEX for 1, 2, or 4 h, and total RNA was isolated and subjected to DNA microarray analysis. Genes whose mRNA expression was increased >2-fold by DEX alone were selected, and their relative mRNA expression levels compared with vehicle-treated cells (0 h) were plotted versus time after treatment with DEX. (*C*) HeLa cells were cotransfected with GRE-Luc, expression plasmids for FLAG-HEXIM1 (FLAG-HEXIM1 +) or empty vector (FLAG-HEXIM1 −), and short interfering RNA against HEXIM1 (siHEXIM1 +) or control vector (siHEXIM1 −), as indicated. After 24 h of treatment with 100 nM DEX, whole-cell extracts were prepared and subjected to luciferase assay and Western blots. (*D*) Human VSMC were transfected with GRE-Luc and cultured in the presence or absence of 5 mM HMBA for 12 h. After 24 h of treatment with 100 nM DEX, whole-cell extracts were prepared and subjected to luciferase assay and Western blots. Tx, treatment; RLU, relative light units.

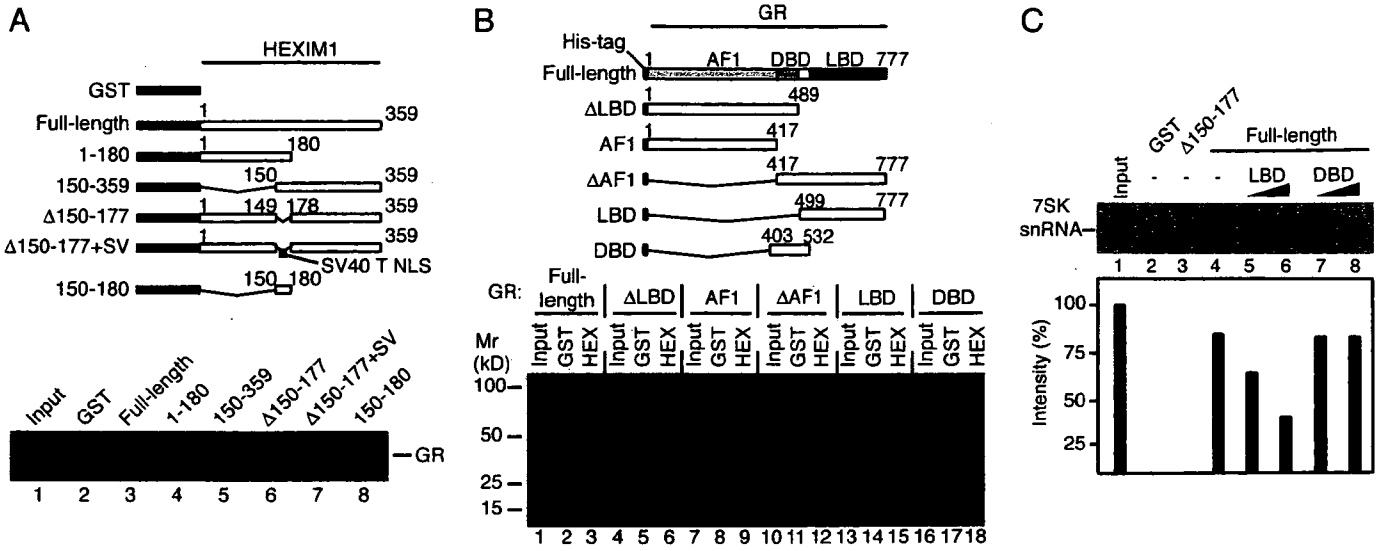

Fig. 3. HEXIM1 directly interacts with GR. (*A* and *B*) GST or GST-fused HEXIM1 mutants were immobilized on glutathione Sepharose beads and incubated with *in vitro*-translated ^{35}S-labeled GR or its mutants, and bound GR was analyzed with SDS/PAGE followed by fluorography. SV40, simian virus 40. (*C*) Four picomoles of GST or GST-fused HEXIM1 mutants were immobilized on glutathione Sepharose beads and incubated with ^{32}P-labeled *in vitro*-transcribed 7SK (lane 1) in the absence or presence of 12 pmol (lanes 5 and 7) or 60 pmol (lanes 6 and 8) of bacterially expressed 6His-GR LBD or DBD as indicated. Bound RNA was analyzed with denaturing PAGE followed by autoradiography. The radioactivity of each band quantified by using Fuji Film BAS2000 image analyzer is shown.

7SK-Binding Domain of HEXIM1 Directly Interacts with GR LBD in a Ligand-Independent Manner. Bacterially expressed GST-HEXIM1 and its various mutants were tested for the interaction with [^{35}S]methionine-labeled *in vitro*-translated full-length GR. Deletion of either N- or C-terminal part of HEXIM1 did not affect binding to GR. However, deletion of the central NLS or its replacement with the simian virus 40 large T-antigen NLS abolished GR binding, and the HEXIM1 NLS alone could strongly bind GR (Fig. 3*A*), indicating that a mere cluster of basic amino acids acting as an NLS is not sufficient and that the native HEXIM1 NLS region is required for binding GR. Next, to identify a HEXIM1-binding domain of GR, bacterially expressed GST-HEXIM1 was immobilized, and *in vitro*-translated 6His-GR or its mutants were applied in the absence of ligand. Either full-length GR, AF1-deleted GR, or the LBD alone could still bind HEXIM1. However, neither AF1 nor DBD was trapped by HEXIM1. Moreover, deletion of the LBD from GR abolished HEXIM1 binding ability, indicating critical requirement of the LBD (Fig. 3*B*). In excellent agreement with this finding, *in vitro* binding of 7SK to HEXIM1 was specifically inhibited by the GR LBD (Fig. 3*C*). Because we obtained similar sets of results when DEX was included in the reactions (data not shown), it is suggested that classical agonists are not critical for the GR–HEXIM1 interaction.

HEXIM1 Interferes with the Interaction Between GR and TIF2. Immunofluorescent analysis revealed that endogenous HEXIM1 constitutively localizes to discrete spots in the nucleus and that ligand-bound GR partially overlaps with HEXIM1 or TIF2 in HeLa cells (Fig. 4*A*). Because HEXIM1 barely colocalized with TIF2 (Fig. 4*A*), we hypothesized that HEXIM1 may compete with TIF2 for binding to GR in a DEX-treated cell nucleus. When HEXIM1 was overexpressed, exogenous expression of TIF2 did not efficiently restore transactivational function of GR (Fig. 4*B*). Moreover, immunoprecipitation of HeLa cell extracts with anti-TIF2 antibody recovered GR but not HEXIM1, and overexpression of HEXIM1 reduced complex formation between GR and TIF2 without significant alteration in the levels of TIF2 (Fig. 4*C*). These results suggest that increase in cellular HEXIM1 down-modulates GR association with TIF2.

Transcription Factor Selectivity of HEXIM1. We next tested the effects of HEXIM1 on AhR, because AhR has been shown to rely on P-TEFb and coactivators, including TIF2, for transcriptional regulation (31, 32). AhR does not directly bind HEXIM1 (data not shown). In HepG2 cell nuclear extracts, adenovirus-mediated overexpression of HEXIM1 did not influence protein levels of either GR or AhR (see Fig. 6, which is published as supporting information on the PNAS web site), and respective ligands increased nuclear fractions of GR and AhR. Transient introduction of antisense deoxyoligonucleotide of 7SK (AS7SK) for disruption of endogenous 7SK (14) resulted in a ≈2.5-fold activation of reporter genes driven by either AhR or GR, indicating the liberation of P-TEFb from 7SK and HEXIM1 to enhance P-TEFb kinase activity. Transactivational activity of AhR and GR was suppressed by HEXIM1 in a dose-dependent manner in the absence of AS7SK. As expected, AS7SK-mediated disruption of 7SK resulted in extinction of HEXIM1 inhibition of AhR. In clear contrast, introduction of AS7SK did not affect the inhibitory effect of HEXIM1 on GR-mediated transcription (Fig. 5), strongly supporting the notion that HEXIM1 suppresses GR-mediated transcription not only through the inhibition of P-TEFb but also by a distinct mechanism that does not involve 7SK. Together, we propose that HEXIM1, by directly binding with GR, may play a distinct role in transcriptional regulation.

Discussion

At this moment, the precise physiological function of HEXIM1 remains unknown. However, genetic disruption of the CLP-1 gene, which is a mouse homologue of HEXIM1, is reported to result in embryonic lethality with marked cardiac hypertrophy (33). Moreover, it is separately shown that hyperactivation of P-TEFb in cardiac myocytes produces cardiac hypertrophy (34). It is therefore likely that HEXIM1 plays an important role in cardiac development and disease pathogenesis. On the other hand, it has been shown that intracellular levels of HEXIM1 are variable and inducible (7, 8). We showed that treatment of VSMC with HMBA resulted in an increase of HEXIM1 expression and a concomitant decrease of GR-activated transcription (8) (see also Fig. 2*D*). Although the role of glucocorticoids in VSMC remains to be clarified, it is likely that

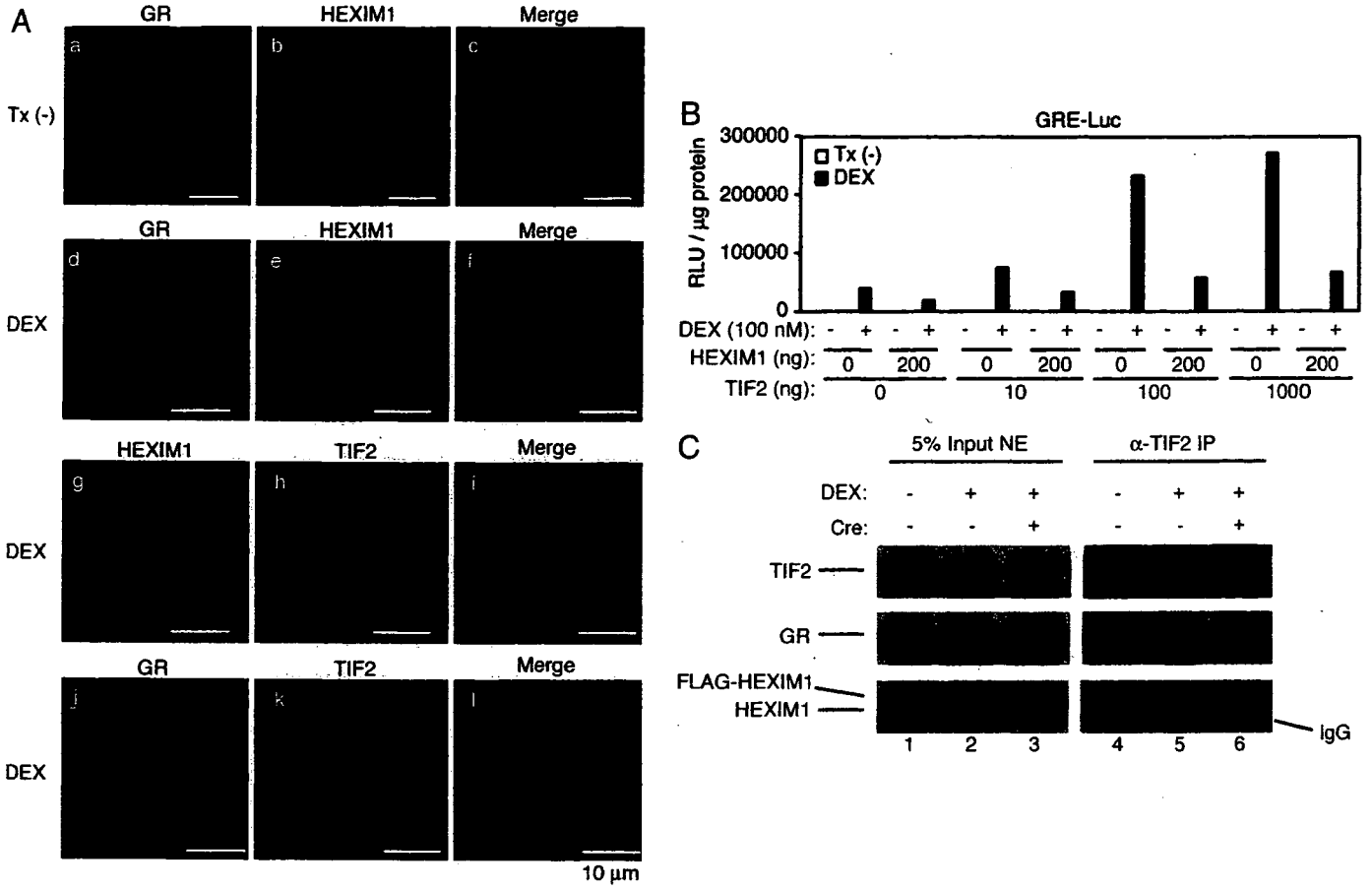

Fig. 4. HEXIM1 represses the functional interaction between GR and TIF2. (*A*) HeLa cells were treated with 100 nM DEX or vehicle [0.1% ethanol, Tx(−)] for 1 h and subjected to indirect immunofluorescence. Confocal laser microscopic images of GR, HEXIM1, and TIF2 are shown. (*B*) COS7 cells were cotransfected with GRE-Luc and expression plasmids for GR, HEXIM1, and TIF2, as indicated. After 24 h of treatment with 100 nM DEX, whole-cell extracts were prepared and subjected to luciferase assay. (*C*) HeLa cells were infected with AdCALNL/FHhHEXIM1 (multiplicity of infection = 30) alone (Cre −) or along with recombinant adenovirus expressing Cre recombinase (Cre +). After 1 h treatment with 1 μM DEX, nuclear extracts (NE) were prepared and immunoprecipitated (IP) with anti-TIF2 antibody. Immunocomplexes were analyzed on Western blots as indicated.

cellular HEXIM1 levels may determine the sensitivity to the hormone in peripheral tissues.

It should be noted that binding of HEXIM1 to 7SK or GR is mediated by the common central arginine-rich motif. The use of the same domain or motif in recognition of nucleic acid and polypeptide molecules is often observed, and two strategies are known to achieve this type of interaction: macromolecular mimicry and induced fit mechanisms (35). The former is observed, for example, in tRNA and polypeptide release factor binding to the same domain of ribosome (36) and in TAFII230 and TATA box element DNA binding to TATA-binding protein (37). The latter is observed in interactions between RNA and arginine-rich motifs (38). The N-terminal part of the HEXIM1 NLS is almost perfectly aligned with the TAR RNA-binding motif of the HIV-1 Tat protein (10). It is known that arginine-rich motifs from different proteins adopt different conformations dependent on the RNA sites recognized and in some cases fold only in the presence of RNA (38). The formation of the Tat/TAR/P-TEFb complex in HIV-infected cells may, therefore, compete and preclude the formation of the inactive

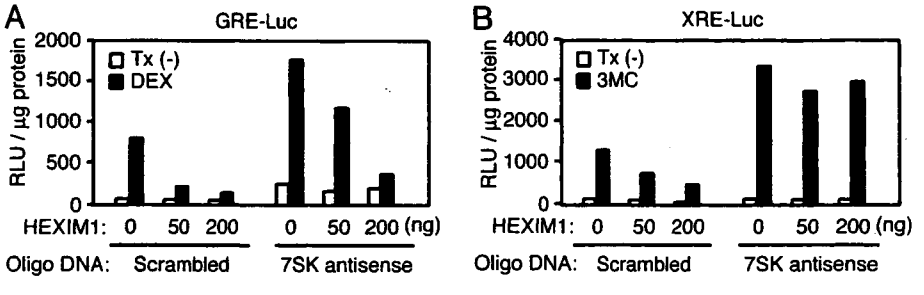

Fig. 5. P-TEFb-dependent and -independent suppression of transcription by HEXIM1. HepG2 cells were cotransfected with the xenobiotic responsive reporter plasmid XRE-Luc or GRE-Luc and indicated amounts of HEXIM1 expression plasmid, along with scrambled or 7SK antisense deoxyoligonucleotides, and treated with 1 μM 3-methylchoranthrene (3MC) or 100 nM DEX for 24 h. Whole-cell extracts were prepared and subjected to luciferase assay. Tx, treatment; RLU, relative light units.

HEXIM1/7SK/P-TEFb complex with resultant activation of the HIV-1 transcription. Because GR also targets the NLS of HEXIM1, it is extremely intriguing to speculate that HEXIM1, by differential formation of distinct protein–protein and protein–RNA complexes through its NLS, modulates cellular gene expression and host defense systems. In this line, it is of particular importance to study how HEXIM1 distinguishes GR and 7SK to form distinct modules. Along this line, continued study is necessary to compare structures of TAR/Tat, HEXIM1/7SK, and HEXIM1/GR and to understand differential roles of HEXIMs in transcriptional regulation in more detail.

In conclusion, we showed that HEXIM1, in addition to the HEXIM1/7SK/P-TEFb complex, specifically binds GR to form a transcriptionally inactive complex. Together with the results of AhR, these data suggest that this mode of complex formation may be restricted to a certain class of transcription factors including GR. HEXIM1 might serve as a molecular device to give distinct biological cues: suppression of transcriptional elongation and repression of GR-mediated transcription.

We thank H. Iba, I. Saito, and T. Wada for material transfer and helpful suggestions and discussion; M. Hasegawa and Y. Tsuboi for technical assistance in mass spectrometric analyses; and Y. Yamaguchi for critical reading of the manuscript. This work was supported in part by grants from the Ministry of Education, Science, Technology, Sports, and Culture; the Ministry of Health, Labour, and Welfare; and the Japan Society for the Promotion of Science. N.S. is a Japan Society for the Promotion of Science Research Fellow.

1. Sims, R. J., III, Mandal, S. S. & Reinberg, D. (2004) *Curr. Opin. Cell Biol.* **16,** 263–271.
2. Woychik, N. A. & Hampsey, M. (2002) *Cell* **108,** 453–463.
3. Kadonaga, J. T. (2004) *Cell* **116,** 247–257.
4. Arndt, K. M. & Kane, C. M. (2003) *Trends Genet.* **19,** 543–550.
5. Hartzog, G. A. (2003) *Curr. Opin. Genet. Dev.* **13,** 119–126.
6. Sims, R. J., III, Belotserkovskaya, R. & Reinberg, D. (2004) *Genes Dev.* **18,** 2437–2468.
7. Kusuhara, M., Nagasaki, K., Kimura, K., Maass, N., Manabe, T., Ishikawa, S., Aikawa, M., Miyazaki, K. & Yamaguchi, K. (1999) *Biomed. Res.* **20,** 273–279.
8. Ouchida, R., Kusuhara, M., Shimizu, N., Hisada, T., Makino, Y., Morimoto, C., Handa, H., Ohsuzu, F. & Tanaka, H. (2003) *Genes Cells* **8,** 95–107.
9. Michels, A. A., Nguyen, V. T., Fraldi, A., Labas, V., Edwards, M., Bonnet, F., Lania, L. & Bensaude, O. (2003) *Mol. Cell Biol.* **23,** 4859–4869.
10. Yik, J. H., Chen, R., Nishimura, R., Jennings, J. L., Link, A. J. & Zhou, Q. (2003) *Mol. Cell* **12,** 971–982.
11. Michels, A. A., Fraldi, A., Li, Q., Adamson, T. E., Bonnet, F., Nguyen, V. T., Sedore, S. C., Price, J. P., Price, D. H., Lania, L. & Bensaude, O. (2004) *EMBO J.* **23,** 2608–2619.
12. Yik, J. H., Chen, R., Pezda, A. C., Samford, C. S. & Zhou, Q. (2004) *Mol. Cell Biol.* **24,** 5094–5105.
13. Nguyen, V. T., Kiss, T., Michels, A. A. & Bensaude, O. (2001) *Nature* **414,** 322–325.
14. Yang, Z., Zhu, Q., Luo, K. & Zhou, Q. (2001) *Nature* **414,** 317–322.
15. Wittmann, B. M., Wang, N. & Montano, M. M. (2003) *Cancer Res.* **63,** 5151–5158.
16. Yik, J. H., Chen, R., Pezda, A. C. & Zhou, Q. (2005) *J. Biol. Chem.* **280,** 16368–16376.
17. Byers, S. A., Price, J. P., Cooper, J. J., Li, Q. & Price, D. H. (2005) *J. Biol. Chem.* **280,** 16360–16367.
18. Beato, M., Herrlich, P. & Schutz, G. (1995) *Cell* **83,** 851–857.
19. Mangelsdorf, D. J., Thummel, C., Beato, M., Herrlich, P., Schutz, G., Umesono, K., Blumberg, B., Kastner, P., Mark, M., Chambon, P., *et al.* (1995) *Cell* **83,** 835–839.
20. Perlmann, T., Rangarajan, P. N., Umesono, K. & Evans, R. M. (1993) *Genes Dev.* **7,** 1411–1422.
21. Yoshikawa, N., Makino, Y., Okamoto, K., Morimoto, C., Makino, I. & Tanaka, H. (2002) *J. Biol. Chem.* **277,** 5529–5540.
22. Kodama, T., Shimizu, N., Yoshikawa, N., Makino, Y., Ouchida, R., Okamoto, K., Hisada, T., Nakamura, H., Morimoto, C. & Tanaka, H. (2003) *J. Biol. Chem.* **278,** 33384–33391.
23. Shimizu, N., Sugimoto, K., Tang, J., Nishi, T., Sato, I., Hiramoto, M., Aizawa, S., Hatakeyama, M., Ohba, R., Hatori, H., *et al.* (2000) *Nat. Biotechnol.* **18,** 877–881.
24. Nishi, T., Shimizu, N., Hiramoto, M., Sato, I., Yamaguchi, Y., Hasegawa, M., Aizawa, S., Tanaka, H., Kataoka, K., Watanabe, H. & Handa, H. (2002) *J. Biol. Chem.* **277,** 44548–44556.
25. Yoshikawa, N., Yamamoto, K., Shimizu, N., Yamada, S., Morimoto, C. & Tanaka, H. (2005) *Mol. Endocrinol.* **19,** 1110–1124.
26. Hiramoto, M., Shimizu, N., Sugimoto, K., Tang, J., Kawakami, Y., Ito, M., Aizawa, S., Tanaka, H., Makino, I. & Handa, H. (1998) *J. Immunol.* **160,** 810–819.
27. Harmer, D., Gilbert, M., Borman, R. & Clark, K. L. (2002) *FEBS Lett.* **532,** 107–110.
28. Duester, G., Farres, J., Felder, M. R., Holmes, R. S., Hoog, J. O., Pares, X., Plapp, B. V., Yin, S. J. & Jornvall, H. (1999) *Biochem. Pharmacol.* **58,** 389–395.
29. Kobayashi, T., Deak, M., Morrice, N. & Cohen, P. (1999) *Biochem. J.* **344 Pt 1,** 189–197.
30. Watanabe, H., Suzuki, A., Goto, M., Ohsako, S., Tohyama, C., Handa, H. & Iguchi, T. (2004) *J. Mol. Endocrinol.* **33,** 763–771.
31. Tian, Y., Ke, S., Chen, M. & Sheng, T. (2003) *J. Biol. Chem.* **278,** 44041–44048.
32. Beischlag, T. V., Wang, S., Rose, D. W., Torchia, J., Reisz-Porszasz, S., Muhammad, K., Nelson, W. E., Probst, M. R., Rosenfeld, M. G. & Hankinson, O. (2002) *Mol. Cell Biol.* **22,** 4319–4333.
33. Huang, F., Wagner, M. & Siddiqui, M. A. (2004) *Mech. Dev.* **121,** 559–572.
34. Sano, M., Abdellatif, M., Oh, H., Xie, M., Bagella, L., Giordano, A., Michael, L. H., DeMayo, F. J. & Schneider, M. D. (2002) *Nat. Med.* **8,** 1310–1317.
35. Nissen, P., Kjeldgaard, M. & Nyborg, J. (2000) *EMBO J.* **19,** 489–495.
36. Song, H., Mugnier, P., Das, A. K., Webb, H. M., Evans, D. R., Tuite, M. F., Hemmings, B. A. & Barford, D. (2000) *Cell* **100,** 311–321.
37. Liu, D., Ishima, R., Tong, K. I., Bagby, S., Kokubo, T., Muhandiram, D. R., Kay, L. E., Nakatani, Y. & Ikura, M. (1998) *Cell* **94,** 573–583.
38. Smith, C. A., Calabro, V. & Frankel, A. D. (2000) *Mol. Cell* **6,** 1067–1076.

CD26 Regulates p38 Mitogen-Activated Protein Kinase–Dependent Phosphorylation of Integrin β_1, Adhesion to Extracellular Matrix, and Tumorigenicity of T-Anaplastic Large Cell Lymphoma Karpas 299

Tsutomu Sato,[1] Tadanori Yamochi,[1] Toshiko Yamochi,[1] Ugur Aytac,[1] Kei Ohnuma,[2] Kathryn S. McKee,[1] Chikao Morimoto,[2] and Nam H. Dang[1]

[1]Department of Lymphoma/Myeloma, University of Texas M.D. Anderson Cancer Center, Houston, Texas and [2]Department of Clinical Immunology, Institute of Medical Science, University of Tokyo, Tokyo, Japan

Abstract

CD26 is an antigen with key role in T-cell biology and is expressed on selected subsets of aggressive T-cell malignancies. To elucidate the role of CD26 in tumor behavior, we examine the effect of CD26 depletion by small interfering RNA transfection of T-anaplastic large cell lymphoma Karpas 299. We show that the resultant CD26-depleted clones lose the ability to adhere to fibronectin and collagen I. Because anti-integrin β_1 blocking antibodies also prevent binding of Karpas 299 to fibronectin and collagen I, we then evaluate the CD26-integrin β_1 association. CD26 depletion does not decrease integrin β_1 expression but leads to dephosphorylation of both integrin β_1 and p38 mitogen-activated protein kinase (MAPK). Moreover, our data showing that the p38MAPK inhibitor SB203580 dephosphorylates integrin β_1 and that binding of the anti-CD26 antibody 202.36 dephosphorylates both p38MAPK and integrin β_1 on Karpas 299, leading to loss of cell adhesion to the extracellular matrix, indicate that CD26 mediates cell adhesion through p38MAPK-dependent phosphorylation of integrin β_1. Finally, *in vivo* experiments show that depletion of CD26 is associated with loss of tumorigenicity and greater survival. Our findings hence suggest that CD26 plays an important role in tumor development and may be a novel therapeutic target for selected neoplasms. (Cancer Res 2005; 65(15): 6950-6)

Introduction

CD26/dipeptidyl peptidase IV is a 110-kDa cell surface glycoprotein that belongs to the serine protease family and is expressed on a variety of tissues, including T lymphocytes, endothelial cells, and epithelial cells. It is composed of a short cytoplasmic domain, a transmembrane region, and an extracellular domain with dipeptidyl peptidase IV activity, which selectively removes the NH_2-terminal dipeptide from polypeptides containing either a proline or an alanine at the penultimate residue. This enzymatic activity seems to regulate the effect of several crucial cytokines and chemokines (1). Work over the past decade has shown CD26 to have an important role in T-cell biology both as a marker of T-cell activation and as a structure associated with key molecules and signaling pathways (2–5).

Requests for reprints: Nam H. Dang, Department of Hematologic Oncology, Nevada Cancer Institute, 10000 West Charleston Boulevard, Suite 260, Las Vegas, NV 89135. Phone: 702-821-0000; Fax: 702-821-0021; E-mail: ndang@nvcancer.org.

Although the role of CD26 in the regulation of normal T-cell physiology has been well characterized, its involvement in tumor biology is still unclear, although early data suggested that it may have a role in the development of selected neoplasms. Studies of patient samples showed that CD26 is highly expressed on lung adenocarcinoma, thyroid carcinoma, and B-cell chronic lymphocytic leukemia (6–8). Meanwhile, CD26 is a marker of aggressive disease for selected subsets of T-cell non-Hodgkin's lymphomas/leukemias. Carbone et al. showed that CD26 expression is restricted to such aggressive types of T-cell malignancies as T-lymphoblastic lymphomas (T-LBL), T-acute lymphoblastic leukemias (T-ALL), and T-anaplastic large cell lymphomas (T-ALCL). Furthermore, multivariate analysis indicated that the expression of CD26 on T-LBL/T-ALL tumor cells is associated with a worse outcome compared with CD26-negative T-LBL/T-ALL tumors (9). Similarly, we showed recently that CD26 expression is a marker of poor prognosis for T-large granular lymphocyte lymphoproliferative disorder (10). Although these findings suggested that CD26 may regulate the malignant behavior of selected tumors, the exact mechanisms involved in the role of CD26 in tumor biology remain to be elucidated.

In this article, we evaluate the role of CD26 in tumor biology by depleting the expression of CD26 on the T-ALCL cell line Karpas 299 with the small interfering RNA (siRNA) technique. We show that CD26 mediates cell adhesion to the extracellular matrix (ECM) proteins fibronectin and collagen I through p38 mitogen-activated protein kinase (MAPK)–dependent phosphorylation of integrin β_1. We also show that CD26 expression regulates topoisomerase IIα level and tumor sensitivity to the topoisomerase II inhibitor doxorubicin. Importantly, loss of CD26 expression on Karpas 299 cells results in decreased tumorigenicity and improved survival in a severe combined immunodeficient (SCID) mouse animal model, hence suggesting that targeting CD26 may be an effective therapeutic approach for selected CD26-positive T-cell malignancies.

Materials and Methods

Reagents. All culture plates and dishes were purchased from Falcon Plastics (Oxnard, CA). Mouse anti-integrin β_1 antibody (P4C10) was from Chemicon (Temecula, CA). Mouse anti-integrin β_1 antibody (4B4) and isotypic control mouse IgG were from Beckman Coulter (Miami, FL). Mouse anti-CD26 antibody (202.36) was from Santa Cruz (Santa Cruz, CA). Mouse anti-CD26 antibodies (1F7 and 5F8) were prepared as described previously (11). Specific inhibitors against p38MAPK SB203580 was from Biomol (Plymouth, Meeting, PA). 3-(4,5-Dimethylthiazol-2-yl)-2,5-diphenyltetrazolium bromide (MTT) was from Sigma (St. Louis, MO). Doxorubicin was from Calbiochem (La Jolla, CA).

Cell culture. The human T-ALCL cell line Karpas 299 was supplied by American Type Culture Collection (Manassas, VA) and maintained in RPMI 1640 (Sigma) with 10% heat-inactivated FCS (Sigma) and antibiotics (100 IU/mL penicillin and 100 μg/mL streptomycin) at 37°C in a humidified atmosphere containing 5% CO_2.

Depletion of CD26. The expression of CD26 was suppressed by Knockout RNAi System (Clontech, Palo Alto, CA) as described previously (12). Briefly, the target sequence ATCATGCATGCAATCAAC, which corresponds to the nucleotide sequence from 1,768 to 1,785 of CD26 cDNA (accession no. NM_001935), was first determined using siDESIGN program at Dharmacon siDESIGN Center (http://design.dharmacon.com/). Complementary oligonucleotides encoding siRNA were then designed and ligated into vector RNAi-Ready pSIREN-RetroQ (Clontech) according to the manufacturer's instructions. Oligonucleotides encoding missense siRNA, in which the target sequence was replaced with the missense sequence ATC*T*TGCA*A*GCAA*A*CAAC, were also ligated into the vector as controls. For the retroviral packaging, these constructs were cotransfected with p10A1 (Clontech) into GP2-293 cells (Clontech) using LipofectAMINE reagent (Invitrogen, Carlsbad, CA). The supernatants containing retrovirus were collected 72 hours after the transfection. Then, this supernatant was added to culture medium of Karpas 299 cells, which was supplemented with 8 μg/mL polybrene (Sigma). After 3 days of incubation, the cells were cultured with 0.4 μg/mL puromycin (Clontech) to eliminate nontransfected cells. Isolated clones were obtained by the standard limiting dilution method.

3-(4,5-Dimethylthiazol-2-yl)-2,5-diphenyltetrazolium bromideassay. The cells were cultured with 100 or 300 μL medium in each well of a 96- or 24-well plate, respectively. To quantify the total number of cells, a quarter volume of the MTT solution, PBS containing 5 mg/mL MTT, was added to the culture medium. To quantify the number of adhesive cells, the culture medium, in which nonadhesive cells were floating after the plates were shaken orbitally several times, was discarded. Then, the same volume of fresh medium with a quarter volume of MTT solution was added to the remaining adhesive cells. In both quantifications, the cells were cultured for 2 hours and added with the same volume of lysis buffer as described previously (13). After overnight incubation at 37°C, the absorbance of dissolved blue formazan was measured at 570 nm in spectrophotometer μQuant (Bio-Tek, Winooski, VT) with KC junior software.

Flow cytometry. The cells were collected, washed twice with PBS, and resuspended in 0.5 mL fluorescence-activated cell sorting buffer, PBS containing 0.5 mmol/L EDTA and 1% (w/v) bovine serum albumin (Sigma). Then, the cells were incubated on ice for 30 minutes with anti-CD26 (Caltag, Burlingame, CA) or anti-integrin β_1 (4B4) mouse monoclonal antibody. Isotypic mouse IgG was used as a control. Surface antigens detected by these antibodies were visualized with FITC-conjugated anti-mouse IgG antibody (Pierce, Rockford, IL), followed by the use of FACSCalibur (Becton Dickinson, San Jose, CA) with CellQuest software.

Western blotting. Cells (1×10^7) were collected, washed twice with PBS, and resuspended in 0.3 mL lysis buffer [1% SDS, 10 mmol/L Tris-HCl (pH 7.4), 10 μg/mL leupeptin, 10 μg/mL aprotinin, 2 mmol/L phenylmethylsulfonyl fluoride] and then boiled for 5 minutes. After passage through a 20-gauge needle 10 times and centrifugation at 15,000 rpm for 20 minutes, the aliquot was boiled again with a standard 4× SDS loading buffer containing 15% (v/v) 2-mercaptoethanol for 5 minutes; 10 μL of which were then subjected to SDS-polyacrylamide gel for electrophoresis followed by the transfer to Immobilon membrane (Millipore, Bedford, MA). The membrane was hybridized with goat anti-CD26/dipeptidyl peptidase IV (R&D, Minneapolis, MN), mouse anti-topoisomerase IIα (Ki-S1, Chemicon), mouse anti-phosphotopoisomerase IIα Thr[1342] (3D4, MBL, Nagoya Japan), goat anti-integrin β_1 L-16 (Santa Cruz), rabbit anti-integrin β_1 pSer[785] (Biosource, Camarillo, CA), rabbit anti-p38MAPK (Cell Signaling, Beverly, MA), or rabbit anti-phospho-p38MAPK Thr[180]/Tyr[182] (Cell Signaling) antibodies. Proteins detected by these antibodies were visualized with horseradish peroxidase–conjugated anti-mouse (DAKOCytomation, Kyoto, Japan), rabbit (Bio-Rad, Hercules, CA), or goat (DAKOCytomation) antibody followed by the use of SuperSignal West Pico Stable Peroxidase Solution (Pierce).

***In vivo* experiments.** Three-week-old female CB-17 SCID mice were purchased from Taconic Farms (Germantown, NY). The mice were kept in laminar flow rooms at constant temperature and humidity. They had free access to food and water. Experimental protocols were approved by the Institutional Ethics Committee for Animal Experimentation. Briefly, every

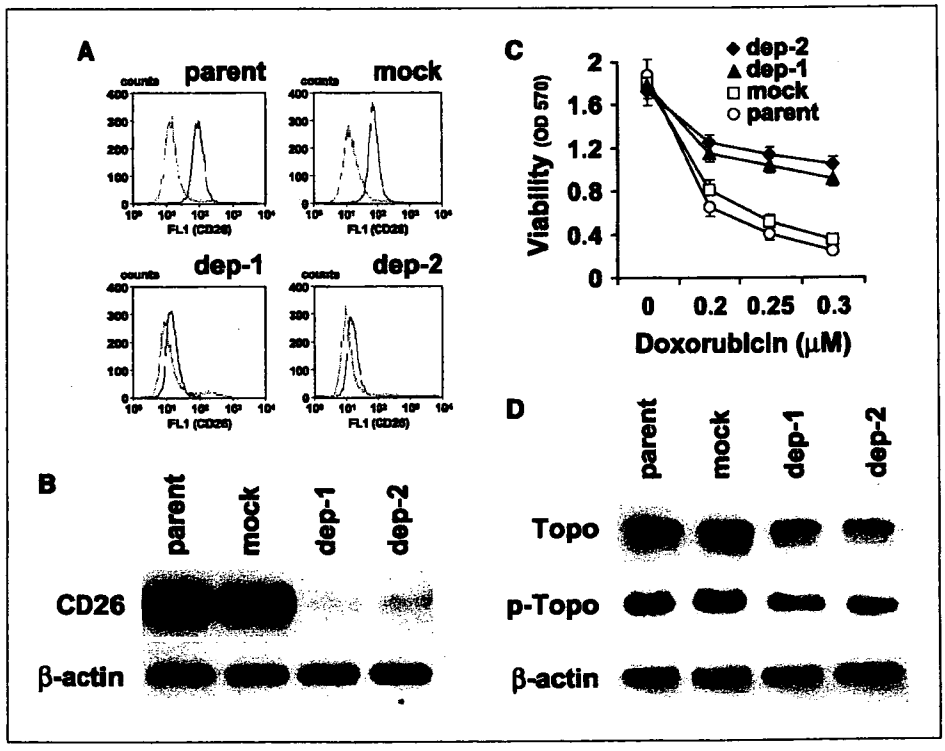

Figure 1. Effect of CD26 depletion on topoisomerase IIα expression and sensitivity to doxorubicin. Karpas 299 cells (parent) were retrovirally transfected with siRNA against CD26. The clones selected by the standard limiting dilution method were designated CD26-depleted clone 1 (dep-1) and clone 2 (dep-2). The control was a clone transfected with missense siRNA (mock). The expression of CD26 was examined by flow cytometry (*A*) and Western blotting (*B*). *A*, *solid lines* or *broken lines*, cells treated with anti-CD26 antibody or isotype control IgG, respectively. *B*, equal amount of proteins was loaded in each lane, with β-actin as control. *C*, Karpas 299 cells (parent, ○), mock (□), and CD26-depleted clones (dep-1, ▲; dep-2, ♦) were plated onto 96-well culture plate (2×10^4 cells per well) and cultured with the indicated concentrations of doxorubicin for 3 days. Following the incubation period, the number of total cell was quantified by MTT assay as described in Materials and Methods. *Points*, mean of five separate experiments ($n = 5$); *bars*, SD. *D*, topoisomerase IIα (*Topo*) and phosphorylated topoisomerase IIα at Thr[1342] (*p-Topo*) of Karpas 299 cells (parent), mock, and CD26-depleted clones (dep-1 and dep-2) were evaluated by Western blotting as described in Materials and Methods, with each lane being loaded with equal amount of proteins and with β-actin as control.

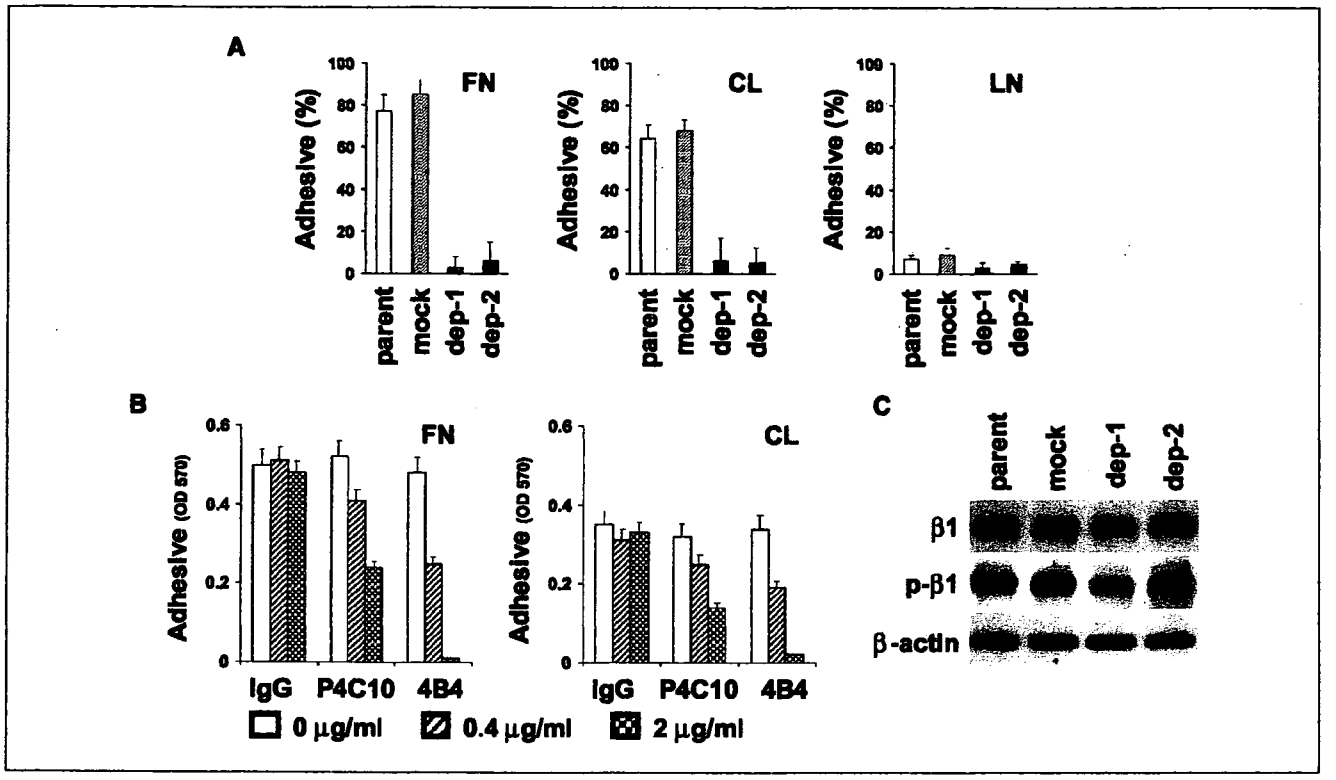

Figure 2. Effect of CD26 depletion on cell adhesion to ECM and integrin β_1 phosphorylation. *A*, Karpas 299 cells (parent; *open columns*), mock (*shaded columns*), and CD26-depleted clones (dep-1 and dep-2; *closed columns*) were plated onto 60 mm dishes (3×10^5 cells per dish) coated with fibronectin (*FN*), collagen I (*CL*), or laminin (*LN*) and cultured for 3 hours. Then, nonadhesive and adhesive cells were separately collected and counted using a hemocytometer. Adhesive cells (%): adhesive cells / adhesive cells + nonadhesive cells. *Columns*, mean of five separate experiments ($n = 5$); *bars*, SD. *B*, Karpas 299 cells were preincubated with 0 (*open columns*), 0.4 (*shaded columns*), or 2 (*hatched columns*) μg/mL blocking antibodies against integrin β_1 (P4C10 or 4B4) for 30 minutes at room temperature. The cells were then plated onto 24-well plates (3×10^5 cells per well) coated with fibronectin or collagen I and placed at room temperature for 1 hour. Following washing of plates to discard nonadhesive cells, the number of adhesive cells remaining was then quantified by MTT assay as described in Materials and Methods. Cells preincubated with isotype control IgG were used as control. *Columns*, mean of five separate experiments ($n = 5$); *bars*, SD. *C*, expression of integrin β_1 (*β1*) and phosphorylated integrin β_1 at Ser^{785} (*p-β1*) on Karpas 299 cells (parent), mock, and CD26-depleted clones (dep-1 and dep-2) was examined by Western blotting as described in Materials and Methods, with equal amount of proteins being loaded in each lane and with β-actin as control.

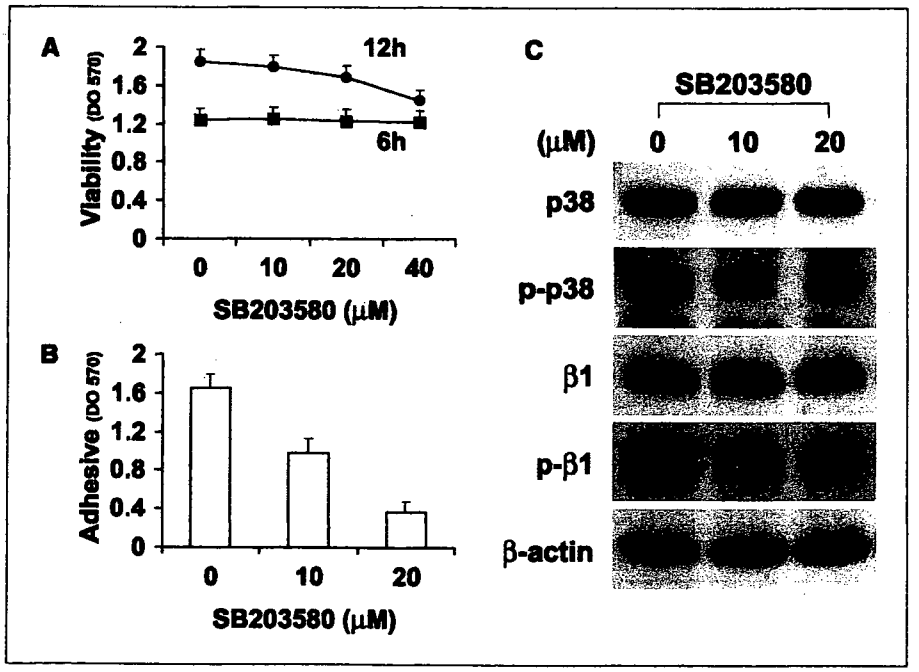

Figure 3. Effect of the p38MAPK inhibitor SB203580 on integrin β_1 phosphorylation. Karpas 299 cells were initially cultured in 24-well plates (3×10^5 cells per well; *A* and *B*) or 10 cm dish (1×10^7 cells per dish; *C*) coated with fibronectin for 6 hours. The cells were then incubated with the indicated concentrations of the p38MAPK inhibitor SB203580 dissolved in DMSO. A final DMSO concentration of 0.4% (v/v) was achieved equally in all samples. *A*, following incubation with SB203580 at 6 (■) or 12 (●) hours, MTT assays were then done as described in Materials and Methods to determine cell viability. *Points*, mean of five separate experiments ($n = 5$); *bars*, SD. *B*, following incubation with SB203580 at 6 hours, plates were washed to discard nonadhesive cells and the number of adhesive cells remaining was quantified by MTT assay as described in Materials and Methods. *Columns*, mean of five separate experiments ($n = 5$); *bars*, SD. *C*, following incubation with SB203580 at 6 hours, levels of p38MAPK (*p38*), phosphorylated p38MAPK at Thr^{180}/Tyr^{182} (*p-p38*), integrin β_1, and phosphorylated integrin β_1 at Ser^{785} were evaluated by Western blotting as described in Materials and Methods, with each lane being loaded with equal amount of proteins and with β-actin as control.

mouse has received i.p. injection of 0.2 mL rabbit anti-asialo-GM1 antisera (Wako Pure Chemical, Osaka, Japan) on day −1. The mice were subsequently divided into three groups, each of which included five animals. Every mouse in each group was then injected i.p. with 0.3×10^6 cells of mock or CD26-depleted clones (dep-1 and dep-2) on day 0. The growth of the palpable tumor in the inguinal regions was followed by measurements with a caliper and its volume was calculated according to the following formula: $MD \times TL^2 \times 1/2$, where MD and TL are the maximum diameter and transverse length, respectively. The mice were sacrificed before the volume of the tumor mass reached 3,000 mm^3 for ethical reason.

Results

Transfection of small interfering RNA against CD26 depletes its expression on Karpas 299 cells. Because CD26 surface expression is associated with aggressive disease in certain types of T-cell malignancies, including T-ALCL (9, 14), we evaluated the role of CD26 in the T-ALCL cell line Karpas 299, which expresses high level of CD26. To deplete CD26 expression, Karpas 299 cells (parent) were retrovirally transfected with siRNA against CD26. Two permanent transfectants were subsequently obtained and designated as CD26-depleted clone 1 (dep-1) and clone 2 (dep-2). The cells transfected with missense siRNA were used as controls (mock). Flow cytometry studies (Fig. 1*A*) and Western blotting analyses (Fig. 1*B*) indicate that CD26 expression is almost completely abrogated on CD26-depleted clones.

CD26 depletion is associated with decreased topoisomerase IIα level and decreased sensitivity to doxorubicin. We showed previously that transfectional overexpression of CD26 results in the up-regulation of topoisomerase IIα expression, associated with enhanced sensitivity to the topoisomerase II inhibitor doxorubicin (12, 15–17). Consistent with our earlier work, our present studies clearly show that CD26 depletion results in decreased doxorubicin sensitivity (Fig. 1*C*). Furthermore, we found that the expression of topoisomerase IIα as well as its phosphorylated active form (18) is down-regulated in CD26-depleted clones (Fig. 1*D*). In contrast, the expression of other structures associated with doxorubicin sensitivity, such as lung resistance protein, multidrug resistance protein-1, and P-glycoprotein, is not influenced by CD26 depletion (data not shown).

CD26 regulates cell adhesion to extracellular matrix through phosphorylation of integrin β_1. CD26 has been described previously to play a role in cell adhesion to the ECM under certain experimental conditions (1, 19). Evaluating the potential effect of CD26 on tumor binding to the ECM, we found that parental Karpas 299 cells and mock clone display greater adhesion to the ECM proteins fibronectin and type I collagen I than CD26-depleted clones (Fig. 2*A*). Because integrins have a well-established role in cell adhesion to ECM proteins, we evaluated the potential association between CD26 and integrin β_1, which is involved in cell adhesion to both fibronectin and collagen I (20). We found that anti–integrin β_1 antibodies significantly block the adhesion of Karpas 299 cells to both fibronectin and collagen I as shown in Fig. 2*B*. Examining further the association between CD26 expression and integrin β_1–dependent cell adhesion, we found no difference in the expression level of integrin β_1 among parental Karpas 299 cells, mock cells, and CD26-depleted clones by flow cytometry (data not shown) and Western blotting (Fig. 2*C*). We next focused on the level of phosphorylated integrin β_1 at residue Ser^{785}, which is necessary for integrin β_1 to function as an adhesion molecule (21). Our findings showed that there is lower level of phosphorylation at integrin β_1 Ser^{785} in CD26-depleted clones than in parental Karpas 299 and mock cells (Fig. 2*C*).

p38MAPK intermediates between CD26 and integrin β_1. We reported recently an association between CD26 and p38MAPK, with overexpression of CD26 resulting in increased p38 phosphorylation at Thr^{180}/Tyr^{182} and depletion of CD26 level leading to decreased p38 phosphorylation at the same residues (12). We therefore examined the possible relationship between p38MAPK and integrin β_1 using the p38MAPK-specific inhibitor SB203580. Although incubation of Karpas 299 cells with SB203580 for 6 hours up to a concentration of 40 μmol/L (Fig. 3*A*) does not lead to decreased cell viability, there is a dose-dependent inhibition of cell adhesion (Fig. 3*B*). In addition, treatment with SB203580 is accompanied by a gradual dephosphorylation of integrin β_1 at Ser^{785} as well as p38MAPK at Thr^{180}/Tyr^{182} (Fig. 3*C*).

Anti-CD26 antibody 202.36 inhibits cell adhesion with dephosphorylation of p38MAPK and integrin β_1. To further delineate CD26 association with p38MAPK and integrin β_1, we

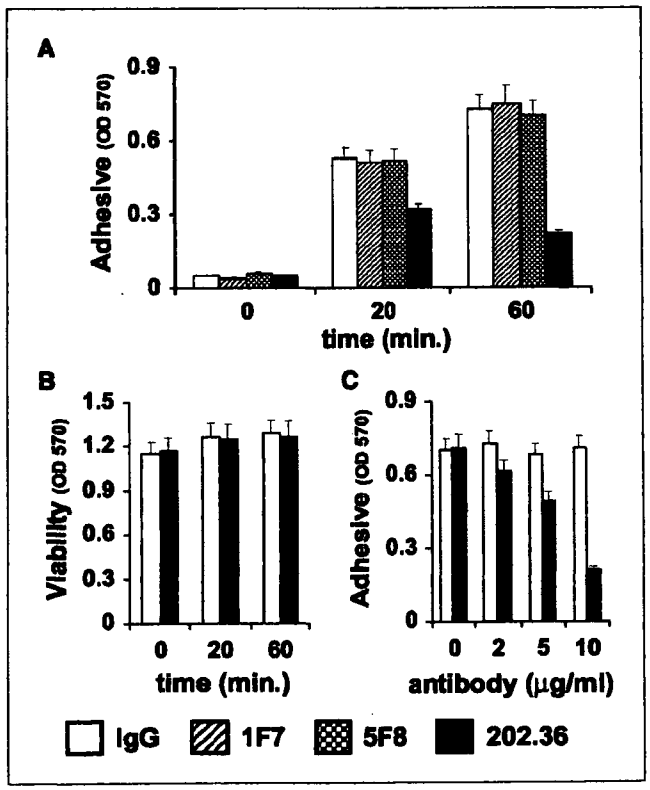

Figure 4. Effect of the anti-CD26 antibody 202.36 on adhesion of Karpas 299 cells to ECM. *A*, Karpas 299 cells were plated onto 24-well plates (3×10^5 cells per well) coated with fibronectin. Shortly thereafter, each antibody (10 μg/mL) was added and the cells were incubated for the indicated times. *Open*, *shaded*, *hatched*, or *closed columns*, isotype control IgG or anti-CD26 antibody clone 1F7, 5F8, or 202.36, respectively. After the incubation period, plates were washed to discard nonadhesive cells and the number of adhesive cells remaining was then quantified by MTT assay as described in Materials and Methods. *B*, cells were treated with 10 μg/mL IgG or 202.36 and incubated for the indicated times. After the incubation period, MTT assays were then done as described in Materials and Methods to determine cell viability. *C*, cells were treated with the indicated concentrations of IgG or 202.36 and incubated for 60 minutes. After the incubation time, plates were washed to discard nonadhesive cells and the number of adhesive cells remaining was then quantified by MTT assay as described in Materials and Methods. *Columns*, mean of five separate experiments ($n = 5$); *bars*, SD (*A-C*).

evaluated the effect of anti-CD26 binding on Karpas 299 cell adhesion to the ECM and p38MAPK and integrin β_1 phosphorylation. We found that the anti-CD26 antibody 202.36 suppresses adhesion of Karpas 299 cells, whereas antibodies recognizing other CD26 epitopes display no inhibitory effect on cell adhesion (Fig. 4*A*). Of note is the fact that 202.36 does not affect cell viability at the dose and time tested (Fig. 4*B*). Furthermore, the inhibitory effect is in a dose-dependent manner (Fig. 4*C*). Importantly, we observed decreased phosphorylation of p38MAPK and integrin β_1 at the Thr^{180}/Tyr^{182} and Ser^{785} residues, respectively, following treatment with the anti-CD26 antibody 202.36 (Fig. 5).

CD26 depletion is associated with decreased tumorigenicity and increased survival in a severe combined immunodeficient mouse model. To investigate the effect of depletion of CD26 expression in an *in vivo* animal model, we inoculated mock and CD26-depleted clones into SCID mice i.p. and then monitored for tumor development and overall survival (Fig. 6). All of the mice inoculated with mock Karpas 299 clones developed tumor masses in the inguinal areas. The largest palpable tumor mass was monitored by serial measurements, and all the mice with tumors were eventually sacrificed per protocol. Importantly, none of the mice inoculated with CD26-depleted clones developed tumor masses over the observed time. Similar studies done with CD26-depleted clone 2 also showed no tumor development over similar times tested (data not shown).

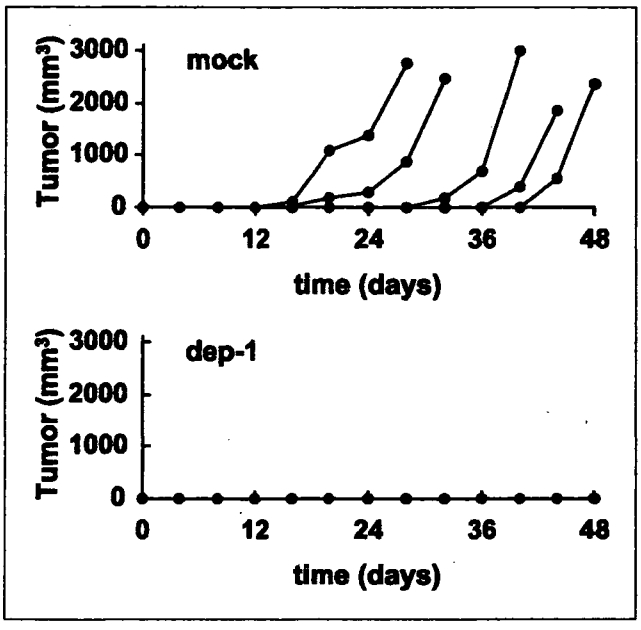

Figure 6. Effect of CD26 depletion on tumorigenicity in an *in vivo* SCID mouse model. SCID mice pretreated with anti–asialo-GM1 antibody were injected i.p. with mock or a CD26-depleted clone dep-1. The maximum diameter (MD) and transverse length (TL) of the largest inguinal mass were measured with a caliper, with tumor volume being calculated by the formula: $MD \times TL^2 \times 1/2$.

Discussion

In this article, we provide evidence linking CD26 to structures with important biological roles. We extend our previous studies by demonstrating the association between CD26 and topoisomerase IIα, with implications for the treatment of selected neoplasms with topoisomerase II inhibitors, such as doxorubicin. Importantly, our study is the first to report a linkage among CD26, p38MAPK, and integrin β_1. Our data indicate that CD26 is associated with integrin-dependent adhesion of Karpas 299 cells to the ECM by regulating p38MAPK-dependent phosphorylation of integrin β_1 at Ser^{785}. In addition, we show that down-regulation of CD26 expression decreases tumorigenicity of Karpas 299 cells in an *in vivo* SCID mouse xenograft model, hence suggesting that targeting CD26 may be an effective therapeutic strategy for selected neoplasms, specifically aggressive hematologic malignancies associated with high level of CD26 expression.

Previous work has suggested that CD26 may have a role in cell adhesion to ECM in selected experimental conditions (19, 22–24), although the mechanism involved with CD26 role in cell adhesion has not been clearly elucidated. Our present findings indicate that

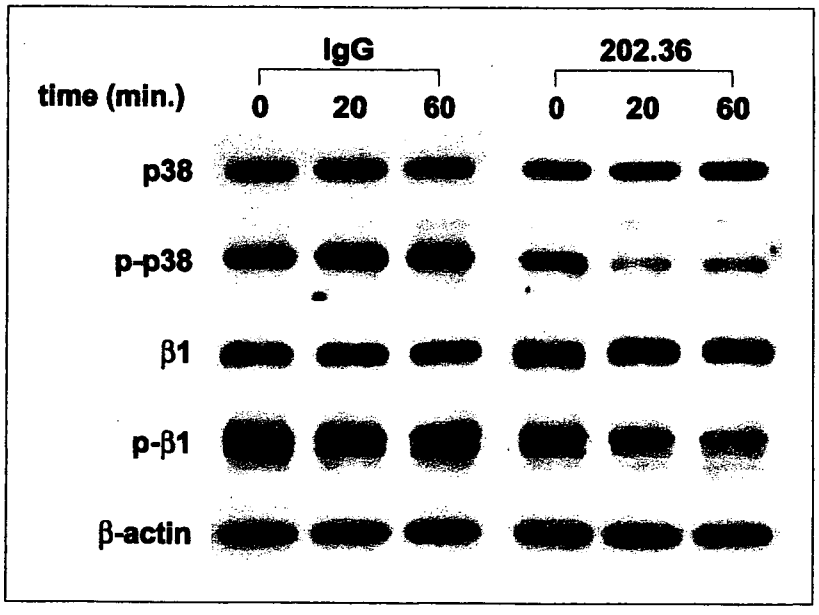

Figure 5. Effect of the anti-CD26 antibody 202.36 on phosphorylation of p38MAPK and integrin β_1. Karpas 299 cells were cultured with 10 μg/mL anti-CD26 antibody 202.36 or isotype control IgG for the indicated times. Levels of p38MAPK, phosphorylated p38MAPK at Thr^{180}/Tyr^{182}, integrin β_1, and phosphorylated integrin β_1 at Ser^{785} were evaluated by Western blotting as described in Materials and Methods, with each lane being loaded with equal amount of proteins and with β-actin as control.

the T-ALCL Karpas 299 cells bind to the ECM proteins fibronectin and collagen I and that this binding is regulated by CD26. Importantly, we show that CD26 affects ECM binding through integrin β_1 as supported by our data demonstrating that treatment with anti-integrin antibody inhibits binding of parental Karpas 299 to ECM and that the anti-CD26 antibody 202.36 also inhibits cell adhesion by suppressing phosphorylation of p38MAPK and integrin β_1 of Karpas 299. Furthermore, depletion of CD26 expression by siRNA transfection results in decreased integrin β_1 phosphorylation and inhibition of cell adhesion to ECM. Our data also suggest that the specific epitope recognized by the anti-CD26 antibody 202.36, which is also the HIV-1 gp120-binding domain of CD26 (25), is responsible for CD26 regulation of cell adhesion, as other anti-CD26 antibodies recognizing other epitopes do not affect ECM binding.

Previous studies showed the importance of phosphorylation of the Ser^{785} residue of integrin β_1 in cell adhesion, as substitution of serine to methionine or aspartate at position 785 results in loss of binding (21). Our work extends these data by demonstrating specifically that the phosphorylation status of integrin β_1 at Ser^{785} regulates integrin β_1–dependent cell adhesion. Of note is the fact that CD26 depletion does not have an effect on the phosphorylation status of integrin β_1 at Thr^{788}/Thr^{789} (data not shown), which has also been reported to regulate integrin β_1–dependent cell adhesion (26, 27). We also note that we consistently observe two bands on Western blotting with the particular antibody used to detect integrin β_1 phosphorylated at Ser^{785}. Although the exact reason for this observation is presently unclear, several potential explanations can be offered. It is possible that particular breakdown products are detected along with the full-length protein. Alternatively, the level of phosphorylation at Ser^{785} residues may differ for different integrin β_1 molecules, hence slightly altering the molecular weights of individual integrin β_1 molecule and resulting in the heterogeneous bands detected. It is also possible that variants of integrin β_1 exist in Karpas 299 cells that are phosphorylated at Ser^{785}, leading to the observation of multiple protein bands.

Our data show that CD26 regulates integrin β_1 phosphorylation of Karpas 299 cells through its effect on p38MAPK. However, the mechanism involved in p38MAPK regulation of the phosphorylation status of integrin β_1 remains to be elucidated. Of note is the fact that transfectional overexpression of CD26 on the human Burkitt B-cell lymphoma cell line Jiyoye results in increased phosphorylation of p38MAPK (12) but does not lead to an accompanying enhancement in phosphorylation of integrin β_1 or induction of cell adhesion (data not shown). It is presently unclear how p38MAPK is able to induce phosphorylation of integrin β_1 in the T-cell lymphoma line Karpas 299 but not in the B-cell lymphoma line Jiyoye cells. It is likely that p38MAPK regulation of integrin β_1 phosphorylation is dependent on other factors that exist in the T-cell line Karpas 299 but not in the B-cell line Jiyoye. Likewise, it is presently unclear as to how CD26 regulates p38 phosphorylation. Given the fact that CD26 is a serine protease capable of cleaving selected biological factors, it is possible that CD26 indirectly regulates p38 phosphorylation pathway via the activity of its cleaved substrates. In addition, because CD26 physically and functionally associates with molecules with key roles in signal transduction, including the tyrosine phosphatase CD45 (5), CD26 may have an effect on p38 phosphorylation through its associated molecules.

An important aim of our present study is to clarify the role of CD26 in regulating the malignant behavior of tumors as a marker of aggressive disease for selected subsets for T-cell malignancies (9, 10, 14), which may allow for the rational selection of CD26 as a potential target for novel therapy. Our *in vivo* data with SCID mouse xenografts conclusively show that depletion of CD26 expression on Karpas 299 cells results in loss of tumorigenicity and enhanced survival. It is likely that the inability to bind to the ECM as a result of CD26 depletion prevents tumor development in the animal model, given the fact that there is no difference in the rate of proliferation or the level of spontaneous cell death between CD26-positive and CD26-depleted Karpas 299 cells (data not shown). Given the fact that Karpas 299 is a T-ALCL cell line, it is interesting to note that in a study involving 8 cases of patients with T-ALCL, 5 of 8 (63%) cases were positive for CD26 expression (9). Taken together, our findings suggest that CD26 ability to regulate cell adhesion through p38MAPK-dependent phosphorylation of integrin β_1 plays a key role in tumorigenicity of the T-ALCL cells Karpas 299 and that treatment strategies targeting CD26 may be an effective therapeutic approach for selected CD26-bearing tumors, including aggressive T-cell malignancies.

Acknowledgments

Received 2/28/2005; revised 5/2/2005; accepted 5/18/2005.

Grant support: Japan Society for the Promotion of Science (T. Sato), Kanae Foundation for Life and Socio-Medical Science (T. Sato), M.D. Anderson Cancer Center Physician-Scientist Award (N.H. Dang), Gillson Longenbaugh Foundation (N.H. Dang), and Goodwin Funds (N.H. Dang).

The costs of publication of this article were defrayed in part by the payment of page charges. This article must therefore be hereby marked *advertisement* in accordance with 18 U.S.C. Section 1734 solely to indicate this fact.

References

1. Pro B, Dang NH. CD26/dipeptidyl peptidase IV and its role in cancer. Histol Histopathol 2004;19:1345–51.
2. Fox DA, Hussey RE, Fitzgerald KA, et al. Tal, a novel 105 KD human T cell activation antigen defined by a monoclonal antibody. J Immunol 1984;133:1250–6.
3. Dang NH, Torimoto Y, Deusch K, Schlossman SF, Morimoto C. Comitogenic effect of solid-phase immobilized anti-1F7 on human CD4 T cell activation via CD3 and CD2 pathways. J Immunol 1990;144:4092–100.
4. Dang NH, Torimoto Y, Sugita K, et al. Cell surface modulation of CD26 by anti-1F7 monoclonal antibody. Analysis of surface expression and human T cell activation. J Immunol 1990;145:3963–71.
5. Torimoto Y, Dang NH, Vivier E, Tanaka T, Schlossman SF, Morimoto C. Coassociation of CD26 (dipeptidyl peptidase IV) with CD45 on the surface of human T lymphocytes. J Immunol 1991;147:2514–7.
6. Asada Y, Aratake Y, Kotani T, et al. Expression of dipeptidyl aminopeptidase IV activity in human lung carcinoma. Histopathology 1993;23:265–70.
7. Aratake Y, Kotani T, Tamura K, et al. Dipeptidyl aminopeptidase IV staining of cytologic preparations to distinguish benign from malignant thyroid diseases. Am J Clin Pathol 1991;96:306–10.
8. Bauvois B, De Meester I, Dumont J, Rouillard D, Zhao HX, Bosmans E. Constitutive expression of CD26/dipeptidylpeptidase IV on peripheral blood B lymphocytes of patients with B chronic lymphocytic leukaemia. Br J Cancer 1999;79:1042–8.
9. Carbone A, Gloghini A, Zagonel V, et al. The expression of CD26 and CD40 ligand is mutually exclusive in human T-cell non-Hodgkin's lymphomas/leukemias. Blood 1995;86:4617–26.
10. Dang NH, Aytac U, Sato K, et al. T-large granular lymphocyte lymphoproliferative disorder: expression of CD26 as a marker of clinically aggressive disease and characterization of marrow inhibition. Br J Haematol 2003;121:857–65.
11. Torimoto Y, Dang NH, Tanaka T, Prado C, Schlossman SF, Morimoto C. Biochemical characterization of CD26 (dipeptidyl peptidase IV): functional comparison of distinct epitopes recognized by various anti-CD26 monoclonal antibodies. Mol Immunol 1992;29:183–92.
12. Yamochi T, Yamochi T, Aytac U, et al. Regulation of p38 phosphorylation and topoisomerase IIα expression in the B-cell lymphoma line Jiyoye by CD26/dipeptidyl peptidase IV (DPPIV), associated with enhanced *in vitro*

and *in vivo* sensitivity to doxorubicin. Cancer Res 2005; 65:1973–83.
13. Hansen MB, Nielsen SE, Berg K. Re-examination and further development of a precise and rapid dye method for measuring cell growth/cell kill. J Immunol Methods 1989;119:203–10.
14. Carbone A, Cozzi M, Gloghini A, Pinto A. CD26/dipeptidyl peptidase IV expression in human lymphomas is restricted to CD30-positive anaplastic large cell and a subset of T-cell non-Hodgkin's lymphomas. Hum Pathol 1994;25:1360–5.
15. Sato K, Aytac U, Yamochi T, et al. CD26/dipeptidyl peptidase IV enhances expression of topoisomerase IIα and sensitivity to apoptosis induced by topoisomerase II inhibitors. Br J Cancer 2003;89:1366–74.
16. Aytac U, Sato K, Yamochi T, et al. Effect of CD26/dipeptidyl peptidase IV on Jurkat sensitivity to G_2-M arrest induced by topoisomerase II inhibitors. Br J Cancer 2003;88:455–62.
17. Aytac U, Claret FX, Ho L, et al. Expression of CD26 and its associated DPPIV enzyme activity enhances sensitivity to doxorubicin-induced cell cycle arrest at G_2-M checkpoint. Cancer Res 2001;61: 7204–10.
18. Ishida R, Iwai M, Marsh KL, et al. Threonine 1342 in human topoisomerase IIα is phosphorylated throughout the cell cycle. J Biol Chem 1996;271: 30077–82.
19. Dang NH, Torimoto Y, Schlossman SF, et al. Human CD4 helper T cell activation: functional involvement of two distinct collagen receptors, 1F7 and VLA integrin family. J Exp Med 1990;172:649–52.
20. Elangbam CS, Qualls CW Jr, Dahlgren RR. Cell adhesion molecules—update. Vet Pathol 1997;34:61–73.
21. Mulrooney JP, Hong T, Grabel LB. Serine 785 phosphorylation of the β_1 cytoplasmic domain modulates β_{1A}-integrin-dependent functions. J Cell Sci 2001; 114:2525–33.
22. Cheng HC, Abdel-Ghany M, Pauli BU. A novel consensus motif in fibronectin mediates dipeptidyl peptidase IV adhesion and metastasis. J Biol Chem 2003;278: 24600–7.
23. Loster K, Zeilinger K, Schuppan D, Reutter W. The cysteine-rich region of dipeptidyl peptidase IV (CD26) is the collagen-binding site. Biochem Biophys Res Commun 1995;217:341–8.
24. Kikkawa F, Kajiyama H, Ino K, Shibata K, Mizutani S. Increased adhesion potency of ovarian carcinoma cells to mesothelial cells by overexpression of dipeptidyl peptidase IV. Int J Cancer 2003;105:779–83.
25. Herrera C, Morimoto C, Blanco J, et al. Comodulation of CXCR4 and CD26 in human lymphocytes. J Biol Chem 2001;276:19532–9.
26. Wennerberg K, Fassler R, Warmegard B, Johansson S. Mutational analysis of the potential phosphorylation sites in the cytoplasmic domain of integrin β_{1A}. Requirement for threonines 788–789 in receptor activation. J Cell Sci 1998;111:1117–26.
27. Stroeken PJ, van Rijthoven EA, Boer E, Geerts D, Roos E. Cytoplasmic domain mutants of β_1 integrin, expressed in β_1-knockout lymphoma cells, have distinct effects on adhesion, invasion and metastasis. Oncogene 2000;19:1232–8.

MOLECULAR AND CELLULAR BIOLOGY, Sept. 2005, p. 7743–7757 Vol. 25, No. 17
0270-7306/05/$08.00+0 doi:10.1128/MCB.25.17.7743–7757.2005

CD26 Mediates Dissociation of Tollip and IRAK-1 from Caveolin-1 and Induces Upregulation of CD86 on Antigen-Presenting Cells

Kei Ohnuma,[1] Tadanori Yamochi,[1,2] Masahiko Uchiyama,[1] Kunika Nishibashi,[1] Satoshi Iwata,[1] Osamu Hosono,[1] Hiroshi Kawasaki,[1] Hirotoshi Tanaka,[1] Nam H. Dang,[2] and Chikao Morimoto[1]*

Department of Clinical Immunology, Advanced Clinical Research Center, Institute of Medical Science, University of Tokyo, 4-6-1 Shirokanedai, Minato-ku, Tokyo 108-8639, Japan,[1] and Department of Lymphoma/Myeloma, M. D. Anderson Cancer Center, 1515 Holcombe Boulevard, Houston, Texas 77030[2]

Received 10 March 2005/Returned for modification 8 April 2005/Accepted 30 May 2005

CD26 is a T-cell costimulatory molecule with dipeptidyl peptidase IV enzyme activity in its extracellular region. We have previously reported that the addition of recombinant soluble CD26 resulted in enhanced proliferation of human T lymphocytes induced by the recall antigen tetanus toxoid (TT) via upregulation of CD86 on monocytes and that caveolin-1 was a binding protein of CD26, and the CD26–caveolin-1 interaction resulted in caveolin-1 phosphorylation (p-cav-1) as well as TT-mediated T-cell proliferation. However, the mechanism involved in this immune enhancement has not yet been elucidated. In the present work, we perform experiments to identify the molecular mechanisms by which p-cav-1 leads directly to the upregulation of CD86. Through proteomic analysis, we identify Tollip (Toll-interacting protein) and IRAK-1 (interleukin-1 receptor-associated serine/threonine kinase 1) as caveolin-1-interacting proteins in monocytes. We also demonstrate that following stimulation by exogenous CD26, Tollip and IRAK-1 dissociate from caveolin-1, and IRAK-1 is then phosphorylated in the cytosol, leading to the upregulation of CD86 via activation of NF-κB. Binding of CD26 to caveolin-1 therefore regulates signaling pathways in antigen-presenting cells to induce antigen-specific T-cell proliferation.

CD26 is a widely distributed 110-kDa cell surface glycoprotein with known dipeptidyl peptidase IV (DPPIV) (EC 3.4.14.5) activity in its extracellular domain (16, 38). This enzyme is capable of cleaving amino-terminal dipeptides with either L-proline or L-alanine at the penultimate position. While CD26 expression is enhanced following activation of resting T cells, $CD4^+$ $CD26^{high}$ T cells respond maximally to recall antigens such as tetanus toxoid (TT) (39). Cross-linking of CD26 and CD3 with solid-phase immobilized monoclonal antibodies (MAbs) can induce T-cell costimulation and interleukin-2 (IL-2) production by either human $CD4^+$ T cells or Jurkat T-cell lines transfected with CD26 cDNA (16, 56). In addition, anti-CD26 antibody treatment of T cells leads to a decrease in the surface expression of CD26 via its internalization, and such modulation results in an enhanced proliferative response to anti-CD3 or anti-CD2 stimulation as well as enhanced tyrosine phosphorylation of signaling molecules such as CD3ζ and p56-Lck (19). Moreover, we showed that DPPIV enzyme activity is required for CD26-mediated T-cell costimulation and various immune responses (23, 45, 58). We have recently shown that internalization of CD26 after cross-linking is mediated in part by the mannose-6-phosphate/insulin-like growth factor II receptor and that the interaction of CD26 and the mannose-6-phosphate/insulin-like growth factor II receptor plays a role in CD26-induced T-cell costimulation (20).

* Corresponding author. Mailing address: Division of Clinical Immunology, Advanced Clinical Research Center, Institute of Medical Science, University of Tokyo, 4-6-1 Shirokanedai, Minato-ku, Tokyo 108-8639, Japan. Phone: 81-354-495-546. Fax: 81-354-495-448. E-mail: morimoto@ims.u-tokyo.ac.jp.

In a recent study, we demonstrated that caveolin-1 is a binding protein of CD26 and that CD26 on activated memory T cells interacts with caveolin-1 on TT-loaded monocytes (43). In this interaction, the scaffolding domain (SCD) of caveolin-1, comprising residues 82 to 101, is associated with the caveolin binding domain (CBD) of CD26, comprising residues 201 to 211. Caveolin-1 was first identified as a major tyrosine-phosphorylated protein in v-Src-transformed chicken embryo fibroblasts (18). Multiple lines of evidence now suggest that caveolin-1 acts as a scaffolding protein capable of directly interacting with and modulating the activity of caveolin-bound signaling molecules. In support of this hypothesis, caveolin-1 binding can functionally modulate the activity of G-protein-coupled protein, membrane protein, nonreceptor tyrosine kinase, and nonreceptor serine/threonine kinases such as H-Ras, Src family kinases, protein kinase C isoforms, epidermal growth factor receptor, and endothelial nitric oxide synthetase (48). Caveolin-1 is the principal structural protein of caveolae and plays a role in the vesicular transport system, including lipid homeostasis, cell cycle regulation, apoptosis, and the regulation of signal transduction pathways (48, 51). In immune cells, caveolin-1 expressed on monocytes/macrophages helps to regulate scavenged lipids (28). Recently, we identified caveolin-1 on antigen-presenting cells (APC) as a binding protein for CD26 and demonstrated that CD26 stimulation upregulates surface expression of CD86 on APC by means of caveolin-1 and enhances TT-mediated T-cell proliferation (43). However, the signaling pathways resulting from CD26-mediated phosphorylation of caveolin-1 (p-cav-1) that lead to the eventual upregulation of CD86 in APC still remain to be elucidated.

In the present paper, we undertook studies to define the

molecular mechanisms by which p-cav-1 leads directly to the upregulation of CD86. We identify Tollip (Toll-interacting protein) and IRAK-1 (IL-1 receptor [IL-1R]-associated serine/threonine kinase 1) as caveolin-1-interacting proteins in APC through proteomic analysis. We demonstrate that binding of exogenous CD26 to APC results in the phosphorylation of caveolin-1 and dissociation of Tollip and IRAK-1 from caveolin-1 in the membrane of APC. Furthermore, following dissociation from caveolin-1 in the cell membrane, IRAK-1 is phosphorylated in the cytoplasm, leading eventually to the upregulation of CD86 through NF-κB activation. CD26 therefore enhances antigen-specific T-cell proliferation by engaging signaling pathways of APC through its interaction with caveolin-1.

MATERIALS AND METHODS

Cells, antibodies, and reagents. HEK293 human embryonal kidney, COS-7 monkey fibroblast, and THP-1 human monocyte cell lines were grown as described previously (43). Human peripheral monocytes were purified from peripheral blood mononuclear cells using a MACS Monocyte Isolation Kit II (Miltenyi), collected from healthy adult volunteers who were immunized with TT within 1 year before donation, and incubated according to the methods described previously (42). Informed consent was obtained from healthy adult volunteers. To avoid the effect of lipopolysaccharide (LPS) contamination, polymyxin B sulfate (20 IU/ml; Sigma-Aldrich) was added in all monocyte-containing cultures.

Anti-caveolin-1 rabbit polyclonal antibody (PAb), anti-IRAK rabbit PAb, anti-IκBα MAb, anti-glutathione-*S*-transferase (GST) MAb, antihemagglutinin (anti-HA) MAb, and anti-HA rabbit PAb agarose-conjugated antibodies were purchased from Santa Cruz Biotechnology Inc.; anti-phospho-caveolin-1 MAb was from BD Transduction; anti-Tollip rat MAb was from ALEXIS Biochemicals; anti-vesicular stomatitis virus (VSV) rabbit PAb was from Medical & Biological Laboratory Co. Ltd.; and anti-FLAG (M2) MAb, 3× FLAG peptide, and poly-L-lysine were from Sigma-Aldrich. Polystyrene latex beads (Molecular Probes) conjugated with recombinant soluble CD26 (rsCD26) were prepared as described previously (42, 43).

Constructions of plasmids. HA–caveolin-1 and caveolin-1–enhanced green fluorescent protein (GFP) were made by inserting caveolin-1 cDNA into pCG-N-BL and pEB6-CAG-EGFP (a kind gift from Yoshihiro Miwa) vectors, respectively (55, 61). A series of caveolin-1 deletion mutants were made by inserting cDNA fragments of mutated caveolin-1 generated by PCR. FLAG-Tollip and VSV–IRAK-1 were made by inserting Tollip cDNA into pFLAG-CMV-2 (Sigma) and pCORON1000 VSV-G (Amersham Biosciences), respectively. GST–caveolin-1 and luciferase chimera of the 5′-flanking region of the human CD86 gene were previously constructed in our laboratory as described elsewhere previously (43). All constructs or cDNA fragments were confirmed by DNA sequencing.

2D-PAGE. The membrane fraction from monocytes stimulated by rsCD26-coated polystyrene beads was extracted with a ReadyPrep protein extraction kit (Bio-Rad) according to the manufacturer's instructions. Membrane proteins were then cleaned up to pellets with a two-dimensional (2D) Clean-Up kit (Bio-Rad) and resuspended in rehydration lysis buffer {8 M urea, 2 M thiourea, 4% 3-[(3-cholamidopropyl)-dimethylammonio]-1-propanesulfonate (CHAPS), 50 mM dithiothreitol, 0.5% ZOOM carrier ampholyte (pH range, 3 to 10) (Invitrogen), 0.002% bromphenol blue} to a final concentration of 1 mg/ml. Wide-range immobilized pH gradient strips (pH 3-10NL; Invitrogen) were rehydrated in 155 μl of rehydration lysis buffer containing 50 μg protein and isoelectric focused at 1,367 V · h on a ZOOM IPGRunner system (Invitrogen). Second-dimension sodium dodecyl sulfate-polyacrylamide gel electrophoresis (SDS-PAGE) was performed using 4 to 12% NuPAGE bis-Tris gels (Invitrogen). Analytical gels were stained with colloidal Coomassie brilliant blue R250. Peptide mass mapping was performed by recording peptide mass fingerprints of typical in-gel digests of the corresponding gel spots using matrix-assisted laser desorption ionization–time of flight mass spectrometry (MALDI-TOF MS) (AXIMA-CFR plus; Shimadzu Biotech) and by subsequently searching the MASCOT database (Matrix Sciences).

Coprecipitation and immunoblotting. To study the interaction among endogenous caveolin-1, Tollip, and IRAK-1, lysates of monocytes were prepared using radioimmunoprecipitation assay lysis buffer as described previously (21, 27, 43). Following preclearing by control immunoglobulins (Igs), immunoprecipitations (IPs) were performed by incubating lysates with specific antibodies followed by the addition of protein G-Sepharose beads. Beads were then submitted to SDS-PAGE and Western blot analysis. To examine the interacting domains with fusion proteins, COS cells were transfected with HA–caveolin-1-, FLAG-Tollip-, and VSV–IRAK-1-expressing plasmids. IPs with these cell lysates and Western blotting were performed as described elsewhere previously (21, 27, 43).

Confocal laser microscopy. For fluorescent microscopy experiments using monocytes, cells were treated and stained according to methods described previously (42, 43). For fluorescent microscopy experiments using HEK293 cells, cells were preincubated in LAB-TEK 4-well chamber slide glass (Nalgen Nunc International). GFP–caveolin-1 or HA–caveolin-1, FLAG-Tollip, and VSV–IRAK-1 constructs were transfected using Lipofectamine 2000 reagent (Invitrogen). Cells were then washed with ice-cold phosphate-buffered saline (PBS), fixed in ice-cold 50% acetone in methanol, and incubated with anti-FLAG (M2) or anti-VSV antibodies. After being washed with ice-cold 5% bovine serum albumin–PBS, cells were stained with specific secondary antibodies, followed by mounting with an Antifade Prolong kit (Molecular Probes).

Luciferase assay. HEK293 cells were used to assay for human CD86 promoter activity following CD26–caveolin-1 interaction with Tollip and IRAK-1. Luciferase enzyme activity was determined using a luminometer (Promega), and relative light units were normalized to the protein amount determined with protein assay reagent according to the manufacturer's instructions (Pierce Biotechnology) (22, 32, 43).

Nuclear protein extraction and DNA-binding protein assay. Nuclear extracts were prepared from purified monocytes with indicated stimulations, and enzyme-linked immunosorbent assay (ELISA)-based DNA-binding protein assays were performed using Mercury TransFactor kits (BD Biosciences) as described previously (43).

siRNA against human Tollip and IRAK-1. We selected two target sequences from positions +186 to +206 (ss1) and +774 to +794 (ss2) downstream of the start codon of human Tollip mRNA (sense 1 small interfering RNA [siRNA] [ss1-siRNA], 5′-AAGTTGGCCAAGAATTACGGCdTdT; sense 2 siRNA [ss2-siRNA], 5′-AACAAGGATCCGCCATCAACdTdT). Moreover, mismatched siRNA (mis-siRNA) at 4 nucleotides was prepared to examine nonspecific effects of siRNA duplexes (mis-siRNA, 5′-UAGTTCGCCAAGTATTACCGCdTdT). siRNA targeting for human IRAK-1 was selected from positions +969 to +989 (ss3) downstream of the start codon of human IRAK-1 mRNA (5′-CCGGGC AATTCAGTTTCTACAdTdT). These selected sequences were also submitted to a BLAST search against the human genome sequence to ensure that only one gene of the human genome was targeted. siRNAs were purchased from QIAGEN. Transfection of siRNA into monocytes was conducted using the HVJ-E vector (GenomeONE; kindly provided by Ihsihara Sangyo Kaisha Ltd.) as described previously (43).

Cell labeling, culture conditions, and flow cytometric analysis. For T-cell proliferation assay, 1×10^6 cells/ml in PBS were labeled with an equal volume of 5 μM carboxyfluorescein diacetate succinimidyl ester according to the manufacturer's instructions (Molecular Probes). Unbound carboxyfluorescein diacetate succinimidyl ester, or the deacetylated form, carboxyfluorescein succinimidyl ester (CFSE), was quenched by the addition of an equal volume of heat-inactivated fetal calf serum. Analysis of cells immediately following CFSE labeling indicates a labeling efficiency that exceeds 99%, and all cells remained labeled for at least a 7-day period during cell culture. The labeled T cells were plated at 1×10^5 cells/well in round-bottomed 96-well microtiter plates with suspension in AIM-V medium (GIBCO), and T-cell activation was achieved by the addition of soluble anti-CD3 antibody (OKT3, 0.05 μg/ml) plus phorbol 12-myristate 13-acetate (PMA) (10 ng/ml), or T cells were plated with 1.0×10^4 cells/well of monocytes from the same donor, which were pretreated with or without TT and siRNA as described above. After a 96-h incubation, T-cell proliferation was analyzed by cell division of the $CD3^+$ subset of CFSE fluorescence using FACSCalibur and CellQuest Pro software (Becton-Dickinson).

Statistics. Student's *t* test was used to determine whether the difference between control and sample was significant (with a P value of <0.05 being significant).

RESULTS

Identification of differential membrane protein expression in CD26-stimulated monocytes. To explore signaling events in TT-loaded monocytes stimulated by CD26, we characterized changes in the expression levels of proteins found in the monocyte membrane. For this purpose, TT-loaded monocytes were

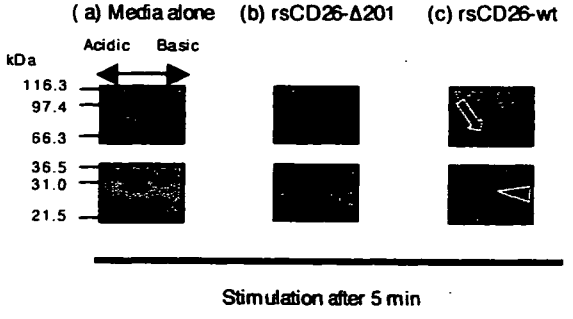

FIG. 1. 2D analysis of membrane proteins extracted from monocytes. Freshly isolated monocytes were pulsed with tetanus toxoid and stimulated with polystyrene latex beads coated with rsCD26-wt or rsCD26 deletion mutant at residues 201 to 211 (rsCD26-Δ201). Following stimulation for 0, 0.5, 5, 10, and 15 min, membrane proteins were extracted from these cells and then separated by 2D-PAGE using pH 3.0-10NL (nonlinear) immobilized pH gradients in the first dimension and 4 to 12% SDS-PAGE and stained with Coomassie brilliant blue 250R. Two spots clearly reduced or disappeared in monocytes undergoing a 5-min stimulation of rsCD26-wt as demonstrated in the figure (arrow and arrow head). Protein spots were identified using MALDI-TOF MS. The protein with a higher molecular mass was determined to be IRAK-1, with the other protein being Tollip. Similar results were obtained in five independent experiments, and the panels shown are the representative results.

stimulated with rsCD26-coated polystyrene latex beads (43). Membrane proteins of TT-loaded monocytes that were either unstimulated or stimulated with wild-type rsCD26 (rsCD26-wt)- or rsCD26-Δ201 (deleting CBD at residues 201 to 210)-coated beads were harvested at various periods and separated by 2D-PAGE as described in Materials and Methods. As shown in Fig. 1, an obvious decrease or disappearance of two spots in 2D-PAGE gel was observed after a 5-min stimulation by rsCD26-wt but not by rsCD26-Δ201. To define the two proteins found to be reduced by rsCD26-wt stimulation, the compatible spots in gels treated with medium alone and rsCD26-Δ201 were excised and analyzed by MALDI-TOF MS for protein identification. Proteins displaying a significant change in response to rsCD26-wt were found to be IRAK-1 (solid arrow in Fig. 1) and Tollip (arrowhead in Fig. 1).

IRAK-1 and Tollip interact with caveolin-1 in the membrane of monocytes. To further determine the protein-protein interaction among caveolin-1, IRAK-1, and Tollip in monocytes, we conducted IP studies using lysates of TT-loaded monocytes. As shown in Fig. 2A, IRAK-1 and caveolin-1 were precipitated with anti-Tollip antibody (lane 2, top and bottom panels). Moreover, Tollip and caveolin-1 were precipitated by anti-IRAK-1 antibody (lane 4, middle and bottom panels). To confirm this interaction, immunocytochemical analysis of monocytes was performed. As shown in Fig. 2B, caveolin-1 was located in the cell surface membrane and perinuclear area of monocytes (panels a and d), and Tollip and IRAK-1 were stained in the cell surface membrane and cytosol (b and g and e and h, respectively). Caveolin-1 and Tollip were colocalized in the cell surface membrane (Fig. 2B, panel c), and caveolin-1 and IRAK-1 were colocalized in the cell surface membrane as well (panel f). Moreover, as reported previously by other investigators (5, 62), Tollip and IRAK-1 were clearly merged with each other (Fig. 2B, panel i). These data strongly suggest that certain numbers of IRAK-1 and Tollip molecules found in monocytes are located in the cell surface membrane with caveolin-1.

We next focused on caveolin-1-mediated signaling events that upregulate CD86 expression following CD26 binding to caveolin-1 on TT-loaded monocytes. As shown in Fig. 2C (panel a), 0.5 to 10 min following stimulation with rsCD26-wt-coated beads, caveolin-1 in the membrane fraction was phosphorylated as reported previously (43). To clarify the comparison of protein expression levels, the changes in intensity of p-cav-1 were shown as a bar graph in Fig. 2C (panel h, solid bars). IRAK-1 and Tollip were found in IP complexes with caveolin-1 PAb at 0- to 0.5-min periods and were dissociated from caveolin-1 at 2 to 10 min following CD26–caveolin-1 interaction (Fig. 2C, panels b and c and light and dark gray bar graphs in panel h, respectively). Of note is that the expression of caveolin-1 was not affected by CD26 stimulation (Fig. 2C, panel d and open bar graphs in panel h). At these time points, IRAK-1 was found to be hyperphosphorylated by Western blot analysis of total lysates (Fig. 2C, panel e). The protein level of Tollip was not changed (Fig. 2C, panel f). In the previous study, we had observed activation of NF-κB in inducing upregulation of CD86 in response to CD26–caveolin-1 interaction (43). We therefore examined the potential involvement of NF-κB in caveolin-1-mediated signaling events that lead to the upregulation of CD86 expression following CD26 binding to caveolin-1 on TT-loaded monocytes. For this purpose, total cell lysates were used to evaluate the degradation of IκBα. As shown in Fig. 2C (panels g and h), IκBα was decreased at 2 to 10 min following CD26–caveolin-1 interaction (dark gray bar graphs in Fig. 2C, panel h). On the other hand, caveolin-1 was not phosphorylated after stimulation with mutant CD26 (rsCD26-Δ201) beads. Similarly, neither release of Tollip nor shift of IRAK was observed (data not shown). These results strongly suggest that the Tollip–IRAK-1–NF-κB cascade was triggered by CD26–caveolin-1 interaction.

Identification of binding domains among caveolin-1, Tollip, and IRAK-1. To further determine the binding domains involved in the caveolin-1–Tollip–IRAK-1 interaction, we constructed a series of GST- or HA-tagged caveolin-1, GST- or FLAG-tagged Tollip, and VSV-tagged IRAK-1 mutants (Fig. 3A). To determine the binding domains involved in the Tollip–caveolin-1 interaction, we first performed a GST pull-down assay using a series of GST-fused caveolin-1 with lysates of THP cells by the same methods described previously (43). As shown in Fig. 3B, Tollip was coprecipitated with GST-tagged wild-type caveolin-1 (GST–Cav-1-wt), Cav-1–N-terminal region (NT)+SCD, and Cav-1–ΔNT (lanes 1, 3, and 5) but not with GST-Cav-NT, Cav-ΔNTΔSCD, and Cav-ΔSCD (lanes 2, 4, and 6), implying that the SCD (residues 82 to 101) of caveolin-1 was required for binding to Tollip. Next, the binding domains of Tollip to caveolin-1 were determined. As shown in Fig. 3C, caveolin-1 was coprecipitated with GST-Tollip-wt, Tollip (protein kinase C conserved region 2 [C2] plus coupling of ubiquitin-conjugation to endoplasmatic reticulum-degradation domain [CUE]), Tollip-ΔCUE, and Tollip-C2 (lanes 1, 2, 3, and 7) but not with GST-Tollip-ΔC2ΔCUE, Tollip-CUE, and Tollip-ΔC2 (lanes 4, 5, and 6). These results revealed that the C2 domain of Tollip (residues 47 to 178) was associated with caveolin-1 interaction. Furthermore, series of FLAG-